

Flexible Vertical Federated Learning with Heterogeneous Parties

Timothy Castiglia, Shiqiang Wang, and Stacy Patterson

Abstract—We propose Flexible Vertical Federated Learning (Flex-VFL), a distributed machine algorithm that trains a smooth, non-convex function in a distributed system with vertically partitioned data. We consider a system with several parties that wish to collaboratively learn a global function. Each party holds a local dataset; the datasets have different features but share the same sample ID space. The parties are heterogeneous in nature: the parties’ operating speeds, local model architectures, and optimizers may be different from one another and, further, they may change over time. To train a global model in such a system, Flex-VFL utilizes a form of parallel block coordinate descent, where parties train a partition of the global model via stochastic coordinate descent. We provide theoretical convergence analysis for Flex-VFL and show that the convergence rate is constrained by the party speeds and local optimizer parameters. We apply this analysis and extend our algorithm to adapt party learning rates in response to changing speeds and local optimizer parameters. Finally, we compare the convergence time of Flex-VFL against synchronous and asynchronous VFL algorithms, as well as illustrate the effectiveness of our adaptive extension.

I. INTRODUCTION

In modern distributed systems, data are often generated by multiple parties and must remain on premises to follow regulations (e.g., GDPR [1], HIPAA [2]) and protect sensitive personal information. Federated learning algorithms [3]–[5] were introduced to provide methods for training machine learning models in distributed systems without the need to share raw data between parties. In these algorithms, data-owning parties train models locally and share intermediate information with a parameter server to update the global model. Federated learning has many important applications including personalized healthcare, smart transportation, and predictive energy systems [4], [6].

Vertical Federated Learning (VFL) is an important class of federated learning. In VFL, parties’ local datasets share a common sample ID space but have different feature sets [5], [7], [8]. This is in contrast to *Horizontal Federated Learning* (HFL), where all parties’ datasets share the same feature space, but each party’s data corresponds to a distinct set of sample IDs [3], [9]–[12]. For example, consider a case where a healthcare provider, insurance company, and wearable device manufacturer wish to collaboratively train a model to identify diseases without directly sharing raw user information with one another [13]. These parties store information about the same people, but each party has a distinct set of information for each individual. In

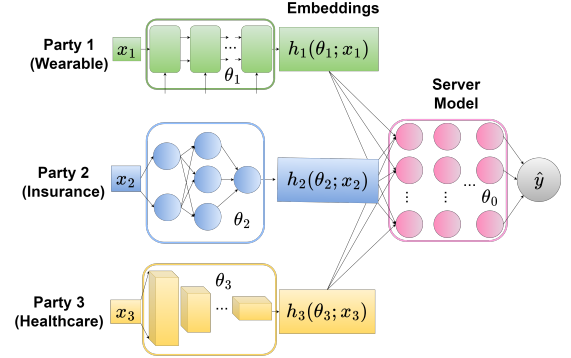


Fig. 1: Example global system model Θ , where party 1’s model θ_1 is an LSTM, party 2’s model θ_2 is an MLP, party 3’s model θ_3 is a CNN, and the server model θ_0 is deep neural network.

VFL, each party typically trains a local feature extractor, while a central server trains a fusion model. The parties periodically exchange intermediate information for updating their local models. We provide an example of a VFL model setup in Figure 1.

Many VFL algorithms assume parties have identical local training: each party uses the same local optimizer to update its model, typically standard SGD [7], [8], [14]–[18]. However, in practice, parties store different types of feature sets ranging from medical images to income values. Centralized machine learning accommodates such multimodal data by supporting different local feature extractors and optimizers for each feature set [19]–[22]. However, such heterogeneous local optimizers have not been accommodated in previous VFL works.

Additionally, it is typically assumed that each party takes the same amount of time to update its local model. The complexity of a party’s model and choice of local optimizer can affect its local training time. There can also be differences in party operating rates due to differing compute capabilities or a varying workload in each party due to colocated jobs. Further, a party’s operating rate may change over time. The slowest parties in the system, the stragglers, can become a bottleneck in the convergence of VFL algorithms [23]–[25].

Previous VFL works have addressed some of these issues. Asynchronous VFL algorithms [14], [16], [26], [27] were proposed as a means to avoid the straggler bottleneck. These algorithms allow parties to train at their own pace, and send updates whenever they are able. However, training with stale information for long periods has been shown to degrade overall model performance, overwhelming the benefits of flexibility to heterogeneous party operating speeds [28], [29]. Some VFL

T. Castiglia and S. Patterson are with the Department of Computer Science, Rensselaer Polytechnic Institute, 110 8th St, Troy, NY 12180 USA, castit@rpi.edu, sep@cs.rpi.edu.

S. Wang is with the IBM Thomas J. Watson Research Center, Yorktown Heights, NY 10598 USA, wangshiq@us.ibm.com.

algorithms using common optimizers other than standard SGD have been proposed [30]–[34], but they require that all parties apply the same local optimizer for training. No previous VFL works incorporate both the effect of time-varying operating speeds and heterogeneous local optimizers.

In this work, we consider a heterogeneous VFL setting where parties have different, time-varying, operating rates and different local optimizers. We seek to answer the following questions. *Is there a method of VFL that can be flexible to the inherently asynchronous nature of distributed parties? Can we analyze the effect of heterogeneous party local optimizers in a VFL setting? And finally, can we generalize the analysis to gain insight into the effect of commonly used local optimizers on VFL convergence?*

To address these questions, we propose Flexible Vertical Federated Learning (Flex-VFL). Flex-VFL is a communication-efficient distributed learning algorithm for vertically partitioned data that is robust to heterogeneous party operating speeds, lets parties utilize different local feature extractors and optimizers, and supports a variety of local optimizers. In Flex-VFL, rather than the server waiting for all parties to complete a given number of local iterations, each party completes as many iterations as possible within a specified timeout. The parties synchronize with the server after this set amount of time has passed. Our approach serves as a middle-ground between fully synchronous and asynchronous methods: training is not slowed down by stragglers, but parties still synchronize regularly to avoid training with stale information for long periods of time. Further, unlike previously proposed VFL algorithms, Flex-VFL allows parties to customize their local optimizers based on their local data and feature extractor architecture.

Flex-VFL is the first theoretically-verified VFL algorithm that has convergence guarantees when parties use different local optimizers. To represent these optimizers in our analysis, we apply arbitrary weights to party gradients at each local iteration. This approach was first introduced by Wang et al. [35], but it has never been applied to the VFL setting or generalized for time-varying optimizer parameters. Our convergence results are generalizable to many variations of VFL, and provides novel insights into the benefits and drawbacks of local momentum [35], proximal terms [36], and variable learning rates on the convergence of VFL algorithms. Specifically, we show that these optimizers improve convergence speed but may increase the error at convergence. Our analysis shows that proper tuning of party learning rates can help offset the error introduced by party heterogeneity.

Our work also provides an adaptive extension to Flex-VFL known as Adaptive Flex-VFL: a meta-optimization algorithm that improves the convergence rate. In systems where other jobs may be colocated on the participating devices, party operating speeds may vary over the course of training. In these cases, it is a challenge to choose hyperparameters to accommodate such heterogeneity over time. Based on our theoretical results on convergence in Flex-VFL, the server can gather party information in each global round to optimize the party learning rates. Adaptive Flex-VFL is designed to be robust to heterogeneous and time-varying party speeds and optimizer parameters.

Our main contributions are as follows:

- 1) We propose Flex-VFL, a Vertical Federated Learning algorithm that is robust to heterogeneous, time-varying parties. Flex-VFL supports a large class of SGD variants such as SGD with local momentum, proximal steps, and variable learning rates.
- 2) We provide convergence analysis for Flex-VFL and show that the error incurred by heterogeneous parties can be offset with the proper choice of learning rates in each round.
- 3) We propose Adaptive Flex-VFL, an extension of Flex-VFL where each party’s learning rate is tailored to its speed and optimizer parameters at each round.
- 4) We experimentally compare Flex-VFL with other VFL algorithms using both simulated and real-world party operating speeds. We find that Flex-VFL outperforms purely synchronous and asynchronous VFL algorithms, reaching target accuracy up to $4\times$ as fast. We also compare Adaptive Flex-VFL and Flex-VFL using real-world time-varying party operating speeds, and show up to a 30% time-to-target improvement.

The rest of the paper is structured as follows. In Section II we discuss related work. Section III introduces our system model and problem formulation. We present Flex-VFL in Section IV. We analyze the convergence of our algorithm in Section V, and present an optimization method to improve convergence speed by adapting party learning rates in Section VI. In Section VII we present our experiments. Finally, we conclude in Section VIII.

II. RELATED WORK

Many works in HFL tackle the challenges of high-latency communication with the use of local iterations. These works analyze the effect of local iterations on convergence [9], [12], [37]. Castiglia et al. [38] and Wang et al. [35] both propose HFL algorithms that support heterogeneous party operating speeds, MLL-SGD [38] and FedNova [35]. FedNova also supports several common local optimizers, such as SGD with proximal steps and local momentum. Both these works provide analysis that give insight into the benefit of supporting these features in federated learning algorithms. However, these previous works in HFL cannot be applied to the VFL case. HFL algorithms rely on distributed gradient descent methods and share model parameter updates, while most VFL algorithms utilize distributed coordinate descent methods and share the output of feature extractors. Thus, the algorithms and analyses for VFL algorithms are fundamentally different.

VFL algorithms are typically variations of coordinate descent methods. Parallel and distributed coordinate descent methods have been proposed [39]–[41], but these works depend on a shared memory structure or data sharing between parties, which is not applicable to the VFL setting. Several works have proposed variants of distributed coordinate descent methods for VFL. Many early works do not include support for multiple local iterations [42]–[44]. Without support for multiple local iterations, progress in optimization is limited by communication time with the server, which can be costly in cases of high communication latency. Some works propose synchronous VFL

TABLE I: Summary of notation used throughout the paper.

Notation	Definitions
K	Number of parties / Number of vertical partitions.
\mathbf{x}_k^i	Local features of data sample i belonging to party k .
\mathbf{X}_k	Local features belonging to party k of all data samples.
y^i	Label for data sample i .
\mathbf{y}	Labels for all data samples.
Θ	Global model parameters.
θ_k	Party k 's local partition of the global model parameters.
$\mathbf{h}_k(\cdot)$	Embedding function for party k .
$l_i(\cdot)$	Loss function on data sample i .
$F(\cdot)$	The objective function.
$\mathbf{g}_k(\cdot)$	Stochastic partial derivative of the objective function with respect to θ_k .
\mathcal{B}	Mini-batch of data samples and their associated labels.
L, L_k	Smoothness parameters for $\nabla_{\Theta} l_i(\cdot)$ and $\nabla_{\theta_k} l_i(\cdot)$, respectively.
σ_k	Variance of party k 's stochastic partial derivatives.
τ_k^r	Number of local iterations taken by party k in round r .
η_k^r	Learning rate for party k in round r .
Φ_{-k}^r	Set of embeddings from all parties in round r except party k .
$w_{k,t}^{r,t}$	Weights on party k 's stochastic partial derivatives at local iteration t and round r .

algorithms that support multiple local iterations [7], [8], [15], [17], [18]. However, these algorithms require all parties to use the same standard SGD local optimizer. Xie et al. [34] propose a synchronous VFL algorithm with multiple local iterations using an ADMM-based optimizer. However, all parties use the same local optimizer in their method, and the fusion network is limited to a linear model, reducing the types of model architectures supported. Additionally, all of these algorithms require that all parties run the same number of local iterations, allowing stragglers to create a bottleneck in training time.

Several works propose asynchronous VFL algorithm [14], [16], [26], [27], but the algorithms do not support multiple local iterations. Additionally, these algorithms only support SGD local updates. Gu et al. [32] and Zhang et al. [33] propose several asynchronous VFL algorithms that support local iterations and common optimizers other than SGD. However, the schemes employed require that each party uses a linear model, which limits the use cases of the proposed algorithms. Their algorithms also do not support parties using different local optimizers in the same algorithm execution.

In contrast with previous work, our work jointly provides support and analyzes the effects of party heterogeneity, time-varying speeds, and limited bandwidth in a VFL setting. Specifically, each party can execute a different number of local iterations in each round, and this number of local iterations can change over time. Further, we provide an analysis of our algorithm that includes the impact of this heterogeneity on the convergence rate and convergence error. These features in our algorithm and analysis allow us to model a more realistic VFL scenario and gives us insight into how to adapt party learning rates to mitigate the error introduced by party heterogeneity.

III. SYSTEM MODEL AND PROBLEM FORMULATION

In this section, we present our system model and problem formulation. We consider a system with a set of parties $\mathcal{K} = \{1, \dots, K\}$. The parties communicate via a central server, forming a hub-and-spoke architecture. The parties and the server may have different operating speeds, and these rates may change over time. We will formalize party operating speeds in Section IV.

Each party k has a local dataset $\mathbf{X}_k \in \mathbb{R}^{N \times D_k}$. We let the i -th row of \mathbf{X}_k be denoted by \mathbf{x}_k^i . We assume that these local datasets are aligned, i.e., \mathbf{x}_k^i and \mathbf{x}_j^i for all parties $k \neq j$ are different features of the same data sample with sample ID i . We let $\mathbf{X} \in \mathbb{R}^{N \times D} = [\mathbf{X}_1, \dots, \mathbf{X}_K]$ where $D = \sum_k D_k$. We can see each \mathbf{X}_k as a vertical partition of \mathbf{X} . Let the i -th data sample be the i -th row in \mathbf{X} , which we denote as \mathbf{x}^i . Let $\mathbf{y} \in \mathbb{R}^{N \times 1}$ be the corresponding labels for the data samples, and let y^i be the label of the i -th data sample. We assume that the parties and server have a copy of the labels \mathbf{y} . We discuss cases where labels are private and only present at a single party in Section IV.

Each party k holds a local model characterized by an *embedding* function $\mathbf{h}_k(\cdot)$ and parameterized by model parameters $\theta_k \in \mathbb{R}^{V_k}$. An embedding function \mathbf{h}_k maps the raw features \mathbf{X}_k to a representation space, typically of lower dimension. For example, \mathbf{h}_k can be a neural network. Each party may have a different model architecture. We let the k -th *embedding* of a data sample \mathbf{x}^i be $\mathbf{h}_k(\theta_k; \mathbf{x}_k^i)$, the output of party k 's feature extractor. If \mathbf{h}_k is a neural network, then an embedding is the output of last layer of the network for single sample. The server stores a *server model* with parameters $\theta_0 \in \mathbb{R}^{V_0}$. The server model is a function of the embeddings from each party and its output is a predicted label \hat{y}_i . We define the *global model* parameters as $\Theta = [\theta_0, \dots, \theta_K] \in \mathbb{R}^V$ where $V = \sum_k V_k$; each θ_k is a *coordinate partition* of Θ . The goal of the parties is to train Θ . We provide an example of the VFL model structure in Figure 1. A benefit of the structure of Θ is that parties can compute partial derivatives of the loss function by exchanging embeddings rather than exchanging their θ_k parameters. Since the size of the embeddings is often much smaller than θ_k , message sizes can be greatly reduced with this structure. Going forward, for simplicity of notation, we may drop \mathbf{x}^i from $\mathbf{h}_k(\cdot)$ when the context is clear.

The VFL objective is to minimize the following function:

$$F(\Theta; \mathbf{X}; \mathbf{y}) := \frac{1}{N} \sum_{i=1}^N l_i(\theta_0; \mathbf{h}_1(\theta_1; \mathbf{x}_1^i); \dots; \mathbf{h}_K(\theta_K; \mathbf{x}_K^i); y^i) \quad (1)$$

where $l_i(\cdot)$ is the loss function for a data sample \mathbf{x}^i and its corresponding label y^i . The loss function $l_i(\cdot)$ measures the error in predicting a label y^i and can be a non-linear function, such as cross-entropy loss, a support vector machine, or a deep neural network, as shown in Figure 1.

Let the partial derivative associated with the coordinate partition θ_k be:

$$\nabla_k F(\Theta; \mathbf{X}; \mathbf{y}) := \frac{1}{N} \sum_{i=1}^N \nabla_{\theta_k} l_i(\theta_0; \mathbf{h}_1(\theta_1; \mathbf{x}_1^i); \dots; \mathbf{h}_K(\theta_K; \mathbf{x}_K^i); y^i).$$

Let \mathcal{B} be a mini-batch of indices of size B corresponding to a subset of rows in \mathbf{X} . We let $\mathbf{X}^{\mathcal{B}}$ be the rows of \mathbf{X} that correspond to a mini-batch \mathcal{B} . Similarly, we let $\mathbf{y}^{\mathcal{B}}$ be the labels that correspond to \mathcal{B} . With some abuse of notation, we define $\mathbf{h}_k(\theta_k; \mathbf{X}_k^{\mathcal{B}})$ to be the set of embeddings for \mathcal{B} for party k .

We denote the stochastic partial derivative of the coordinate partition θ_k as:

$$g_k(\theta_0; \mathbf{h}_1(\theta_1; \mathbf{X}_1^{\mathcal{B}}); \dots; \mathbf{h}_K(\theta_K; \mathbf{X}_K^{\mathcal{B}}); \mathbf{y}^{\mathcal{B}}) := \frac{1}{B} \sum_{i \in \mathcal{B}} \nabla_{\theta_k} l_i(\theta_0; \mathbf{h}_1(\theta_1; \mathbf{x}_1^i); \dots; \mathbf{h}_K(\theta_K; \mathbf{x}_K^i); y^i).$$

With a slight abuse of notation, we let the partial derivatives $g_k(\theta_0; \mathbf{h}_1(\theta_1; \mathbf{X}_1^{\mathcal{B}}); \dots; \mathbf{h}_K(\theta_K; \mathbf{X}_K^{\mathcal{B}}); \mathbf{y}^{\mathcal{B}})$ be equivalently denoted as $g_k(\Theta; \mathcal{B})$. We may drop \mathbf{X} and \mathbf{y} from $F(\cdot)$ and \mathcal{B} from $g_k(\cdot)$ when the context is clear.

We make the following standard assumptions for $l_i(\cdot)$, $F(\cdot)$, and $g_k(\cdot)$ [45]–[47]:

Assumption 1. Smoothness: *There exists positive constants $L < \infty$ and $L_k < \infty$ for $k = 0, \dots, K$ such that for all $\Theta_1 \in \mathbb{R}^V$, $\Theta_2 \in \mathbb{R}^V$:*

$$\|\nabla_{\Theta} l_i(\Theta_1) - \nabla_{\Theta} l_i(\Theta_2)\| \leq L \|\Theta_1 - \Theta_2\| \quad (2)$$

$$\|\nabla_{\theta_k} l_i(\Theta_1) - \nabla_{\theta_k} l_i(\Theta_2)\| \leq L_k \|\Theta_1 - \Theta_2\|. \quad (3)$$

Assumption 2. Unbiased gradients: *For a mini-batch \mathcal{B} , for $k = 0, \dots, K$, the stochastic partial derivatives are unbiased, i.e., for all $\Theta \in \mathbb{R}^V$*

$$\mathbb{E}_{\mathcal{B}} [g_k(\Theta)] = \nabla_{\theta_k} F(\Theta). \quad (4)$$

Assumption 3. Bounded variance: *There exists constants $\sigma_k < \infty$ for $k = 0, \dots, K$ such that the variances of the stochastic partial derivatives are bounded as*

$$\mathbb{E}_{\mathcal{B}} \|\nabla_{\theta_k} F(\Theta) - g_k(\Theta)\|^2 \leq \sigma_k^2 \quad (5)$$

for a mini-batch \mathcal{B} and for all $\Theta \in \mathbb{R}^V$.

Assumption 1 bounds how fast the gradient and partial derivatives can change. Assumption 2 requires that the stochastic partial derivatives computed by each party and the server are unbiased estimates of the full-batch partial derivatives. Assumption 2 can be satisfied in practice by ensuring that sample IDs for a mini-batch are chosen at random. Note, we make no assumption about the distribution of the full dataset \mathbf{X} . Finally, Assumption 3 bounds the variance between the stochastic partial derivatives and full-batch partial derivatives by some constant.

IV. ALGORITHM

We now present Flex-VFL, our algorithm for training a global model with distributed, vertically partitioned data in a system with heterogeneous parties. In each *global round* of Flex-VFL, we employ a type of parallel stochastic block coordinate descent. Each party and the server updates its coordinate partition using its local optimizer for one or more *local iterations*. The parties complete as many of these local iterations as possible before a specified timeout. This differs from synchronous VFL algorithms that wait for all parties to complete the same number of local iterations [7], which can lead to a bottleneck when slow parties are present. We assume that all parties participate in each global round and run at least one local iteration before the given timeout. Flex-VFL runs R global rounds of training.

Algorithm 1 Flexible Vertical Federated Learning

```

1: Initialize:  $\theta_k^{0,0}$  for all parties  $k$  and server model  $\theta_0^{0,0}$ 
2: for  $r \leftarrow 0, \dots, R-1$  do
3:   Select a mini-batch of sample IDs  $\mathcal{B}^r \in \{\mathbf{X}, \mathbf{y}\}$ 
4:   for  $k \leftarrow 1, \dots, K$  in parallel do
5:     Sample features  $\mathbf{X}_k^{\mathcal{B}^r}$  corresponding to IDs in  $\mathcal{B}^r$ 
6:     Send  $\mathbf{h}_k(\theta_k^{r,0}; \mathbf{X}_k^{\mathcal{B}^r})$  to server
7:   end for
8:    $\Phi^r \leftarrow \{\theta_0^{r,0}, \mathbf{h}_1(\theta_1^{r,0}; \mathbf{X}_1^{\mathcal{B}^r}), \dots, \mathbf{h}_K(\theta_K^{r,0}; \mathbf{X}_K^{\mathcal{B}^r})\}$ 
9:   Server sends  $\Phi^r$  to all parties
10:  for  $k \leftarrow 0, \dots, K$  in parallel do
11:     $\triangleright$  Parties and server run until local training timeout
12:    for  $t \leftarrow 0, \dots, \tau_k^r - 1$  do
13:       $\theta_k^{r,t+1} \leftarrow \theta_k^{r,t} - \eta_k^r \mathbf{D}_k(\Phi_{-k}^r; \theta_k^{r,t}, \dots, \theta_K^{r,t}; \mathbf{y}^{\mathcal{B}})$ 
14:    end for
15:     $\theta_k^{r+1,0} \leftarrow \theta_k^{r,\tau_k^r}$ 
16:  end for
17: end for

```

One of the challenges in training for our objective is distributing the necessary information for parties to compute their partial derivatives. For a given data sample \mathbf{x} and its label y , the server must compute:

$$g_0(\Theta; \mathbf{x}) = \nabla_{\theta_0} l(\theta_0; \mathbf{h}_1(\theta_1; \mathbf{x}_1), \dots, \mathbf{h}_K(\theta_K; \mathbf{x}_K); y)$$

and each party k must compute:

$$g_k(\Theta; \mathbf{x}) = \nabla_{\theta_k} l(\theta_0; \mathbf{h}_1(\theta_1; \mathbf{x}_1), \dots, \mathbf{h}_K(\theta_K; \mathbf{x}_K); y) \\ = \nabla_{\theta_k} \mathbf{h}_k(\theta_k)^\top \nabla_{\mathbf{h}_k(\theta_k)} l(\theta_0; \mathbf{h}_1(\theta_1; \mathbf{x}_1), \dots, \mathbf{h}_K(\theta_K; \mathbf{x}_K); y).$$

We can see that for a party to calculate its model update, it needs to first calculate $\nabla_{\mathbf{h}_k(\theta_k)} l(\theta_0; \mathbf{h}_1(\theta_1; \mathbf{x}_1), \dots, \mathbf{h}_K(\theta_K; \mathbf{x}_K); y)$. Thus, to execute multiple local iterations on a data sample \mathbf{x} without communication, each party and the server will need to receive a snapshot of the embeddings $\mathbf{h}_j(\theta_j)$ for all $j \neq k$ and the server model θ_0 at the start of each global round. We describe the process of exchanging this information below. Moving forward, the superscript r, t denotes global round r at local iteration t . We let the snapshot of embeddings for a mini-batch at round r be denoted $\Phi^r = \{\theta_0^{r,0}, \mathbf{h}_1(\theta_1^{r,0}; \mathbf{X}_1^{\mathcal{B}}), \dots, \mathbf{h}_K(\theta_K^{r,0}; \mathbf{X}_K^{\mathcal{B}})\}$.

We describe the training process of Flex-VFL in Algorithm 1. The global model is initialized to $\Theta^{0,0} = [\theta_0^{0,0}, \dots, \theta_K^{0,0}]$. In each global round, the parties agree upon a mini-batch of sample IDs \mathcal{B} on which to train. For example, the server may assign the same random number generator seed to all parties, ensuring each party chooses the same sample IDs at the start of each round. Each party then determines its set of local features $\mathbf{X}_k^{\mathcal{B}}$ that it will use to compute embeddings. Each party, excluding the server, computes its embeddings for the mini-batch, $\mathbf{h}_k(\theta_k; \mathbf{X}_k^{\mathcal{B}})$. These embeddings are sent to the server, and the server distributes its current model θ_0 and Φ^r to all parties.

Next, each party and the server start the *local training period*. Each party and the server run as many local gradient descent steps as it can within a timeout that is pre-specified before training begins. We let τ_k^r be the number of local gradient

descent steps that party k completes in round r , with $1 \leq \tau_k^r < \infty$. This number of local iterations τ_k^r depends on party k 's operating speed in global round r and the local training timeout. Slower parties have smaller τ_k^r values, while faster parties have larger τ_k^r values. Since computation loads may change over time, a party's operating speed, and thus its τ_k^r , may change between each global round. Note that during local iterations, each party only updates its own embedding $\mathbf{h}_k(\boldsymbol{\theta}_k^{r,t})$, and uses stale versions of $\mathbf{h}_j(\boldsymbol{\theta}_j^{r,0})$ for all $j \neq k$. Each party also reuses the same mini-batch for τ_k^r iterations, saving on communication of a new set of embeddings at each local iteration. We show in Section V that the model converges, even though this stale information is used.

A party k 's updates during each local iteration are defined as follows:

$$\boldsymbol{\theta}_k^{r,t+1} = \boldsymbol{\theta}_k^{r,t} - \eta_k^r \mathbf{D}_k \left(\Phi_{-k}^r; \boldsymbol{\theta}_k^{r,0}, \dots, \boldsymbol{\theta}_k^{r,t}; \mathbf{y}^B \right) \quad (6)$$

where Φ_{-k}^r is the set of all embeddings except those from party k , and $\mathbf{D}_k(\cdot)$ is the local optimizer update rule based on the stochastic partial derivatives from the start of the global round to the current local iteration. The cumulative update to each local model over a set of local iterations is as follows:

$$\boldsymbol{\theta}_k^{r,\tau_k^r} = \boldsymbol{\theta}_k^{r,0} - \eta_k^r \sum_{t=0}^{\tau_k^r-1} \mathbf{D}_k \left(\Phi_{-k}^r; \boldsymbol{\theta}_k^{r,0}, \dots, \boldsymbol{\theta}_k^{r,t}; \mathbf{y}^B \right) \quad (7)$$

We assume that the cumulative update over all local iterations can be rewritten in the following form:

$$\sum_{t=0}^{\tau_k^r-1} \mathbf{D}_k \left(\Phi_{-k}^r; \boldsymbol{\theta}_k^{r,0}, \dots, \boldsymbol{\theta}_k^{r,t}; \mathbf{y}^B \right) := \sum_{t=0}^{\tau_k^r-1} w_k^{r,t} \mathbf{g}_k(\Phi_{-k}^r; \mathbf{h}_k(\boldsymbol{\theta}_k^{r,t}); \mathbf{y}^B) \quad (8)$$

where $w_k^{r,t} \geq 1$ are weights applied to each gradient update. Note that we do not assume that each index of these sums in (8) are equivalent. By rewriting party update rules in this way, we can analyze a variety of common local optimizers. Below, we present some examples of common local optimizers whose updates can be written in the form of (8).

- **Classical SGD:** In classical SGD, our update rule is:

$$\mathbf{D}_k \left(\Phi_{-k}^r; \boldsymbol{\theta}_k^{r,0}, \dots, \boldsymbol{\theta}_k^{r,t}; \mathbf{y}^B \right) := \mathbf{g}_k(\Phi_{-k}^r; \mathbf{h}_k(\boldsymbol{\theta}_k^{r,t}); \mathbf{y}^B).$$

By setting $w_k^{r,t} = 1$ for all parties, rounds, and local iterations in (8), our update rule becomes classical SGD.

- **SGD with Momentum:** SGD with local momentum is where a party resets its momentum buffer to zero at the start of each global round. The update rule for SGD with local momentum is defined as follows:

$$\mathbf{D}_k \left(\Phi_{-k}^r; \boldsymbol{\theta}_k^{r,0}, \dots, \boldsymbol{\theta}_k^{r,t}; \mathbf{y}^B \right) := \mathbf{u}_k^{r,t}$$

where

$$\begin{aligned} \mathbf{u}_k^{r,0} &= \mathbf{g}_k(\Phi_{-k}^r; \mathbf{h}_k(\boldsymbol{\theta}_k^{r,0})) \\ \mathbf{u}_k^{r,t} &= \rho \mathbf{u}_k^{r,t-1} + \mathbf{g}_k(\Phi_{-k}^r; \mathbf{h}_k(\boldsymbol{\theta}_k^{r,t})) \end{aligned}$$

where ρ is a tunable parameter. The updates $\mathbf{u}_k^{r,t}$ at each local iteration t can be defined as follows:

$$\begin{aligned} \mathbf{u}_k^{r,t} &= \rho \mathbf{u}_k^{r,t-1} + \mathbf{g}_k(\Phi_{-k}^r; \mathbf{h}_k(\boldsymbol{\theta}_k^{r,t-1})) \\ &= \rho^2 \mathbf{u}_k^{r,t-2} + \rho \mathbf{g}_k(\Phi_{-k}^r; \mathbf{h}_k(\boldsymbol{\theta}_k^{r,t-2})) \\ &\quad + \mathbf{g}_k(\Phi_{-k}^r; \mathbf{h}_k(\boldsymbol{\theta}_k^{r,t-1})) \\ &= \sum_{s=0}^{t-1} \rho^{t-1-s} \mathbf{g}_k(\Phi_{-k}^r; \mathbf{h}_k(\boldsymbol{\theta}_k^{r,s})). \end{aligned}$$

Plugging this into (6), we have:

$$\begin{aligned} \boldsymbol{\theta}_k^{r,t} &= \boldsymbol{\theta}_k^{r,t-1} - \eta_k^r \sum_{s=0}^{t-1} \rho^{t-1-s} \mathbf{g}_k(\Phi_{-k}^r; \mathbf{h}_k(\boldsymbol{\theta}_k^{r,s})) \\ &= \boldsymbol{\theta}_k^{r,t-2} - \eta_k^r \sum_{s=0}^{t-2} \rho^{t-2-s} \mathbf{g}_k(\Phi_{-k}^r; \mathbf{h}_k(\boldsymbol{\theta}_k^{r,s})) \\ &\quad - \eta_k^r \sum_{s=0}^{t-1} \rho^{t-1-s} \mathbf{g}_k(\Phi_{-k}^r; \mathbf{h}_k(\boldsymbol{\theta}_k^{r,s})). \end{aligned}$$

Applying this recursion to our update rule in (7), we have:

$$\boldsymbol{\theta}_k^{r,\tau_k^r} = \boldsymbol{\theta}_k^{r,0} - \eta_k^r \sum_{t=0}^{\tau_k^r-1} \sum_{s=0}^t \rho^{t-s} \mathbf{g}_k(\Phi_{-k}^r; \mathbf{h}_k(\boldsymbol{\theta}_k^{r,s})).$$

Thus, in order to represent local momentum, the weights in (8) can be set as follows:

$$w_k^{r,t} = 1 + \rho + \rho^2 + \dots + \rho^{\tau_k^r-1-t} = \frac{1 - \rho^{\tau_k^r-t}}{1 - \rho}.$$

- **Proximal updates:** As first proposed in FedProx [36], and first applied to a VFL algorithm by Liu et al. [7], one can apply a proximal term by defining a party's update rule as follows:

$$\begin{aligned} \mathbf{D}_k \left(\Phi_{-k}^r; \boldsymbol{\theta}_k^{r,0}, \dots, \boldsymbol{\theta}_k^{r,t}; \mathbf{y}^B \right) &:= \\ &\mathbf{g}_k(\Phi_{-k}^r; \mathbf{h}_k(\boldsymbol{\theta}_k^{r,t})) + \mu \left(\boldsymbol{\theta}_k^{r,t} - \boldsymbol{\theta}_k^{r,0} \right) \end{aligned}$$

where μ is a tunable parameter. Plugging this into (6) we have:

$$\boldsymbol{\theta}_k^{r,t+1} = \boldsymbol{\theta}_k^{r,t} - \eta_k^r \left(\mathbf{g}_k(\Phi_{-k}^r; \mathbf{h}_k(\boldsymbol{\theta}_k^{r,t})) + \mu \left(\boldsymbol{\theta}_k^{r,t} - \boldsymbol{\theta}_k^{r,0} \right) \right)$$

Subtracting $\boldsymbol{\theta}_k^{r,0}$ from both sides we have:

$$\begin{aligned} \boldsymbol{\theta}_k^{r,t+1} - \boldsymbol{\theta}_k^{r,0} &= (1 - \eta_k^r \mu) \left(\boldsymbol{\theta}_k^{r,t} - \boldsymbol{\theta}_k^{r,0} \right) \\ &\quad - \eta_k^r \mathbf{g}_k(\Phi_{-k}^r; \mathbf{h}_k(\boldsymbol{\theta}_k^{r,t})). \end{aligned}$$

Repeatedly applying the recursion on $\boldsymbol{\theta}_k^{r,t}$, we have:

$$\boldsymbol{\theta}_k^{r,t+1} - \boldsymbol{\theta}_k^{r,0} = -\eta_k^r \sum_{t=0}^{\tau_k^r-1} (1 - \eta_k^r \mu)^{\tau_k^r-1-t} \mathbf{g}_k(\Phi_{-k}^r; \mathbf{h}_k(\boldsymbol{\theta}_k^{r,t})).$$

Thus, the weights in (8) can be set as follows to represent proximal steps in VFL:

$$w_k^{r,t} = (1 - \eta_k^r \mu)^{\tau_k^r-t-1}.$$

This method of generalizing to several local optimizers was first shown in the context of HFL by Wang et al. [35]. However

it has yet to be analyzed in the context of VFL, which provides its own unique challenges. We discuss this more in Section V.

Communication cost: The size of messages in Flex-VFL is of note. For each party to compute its partial derivative, every party must exchange its embeddings for the current mini-batch, and the server must send its model θ_0 to the parties. Let the size of the k -th embedding for a single data sample be O_k . The total amount of data sent per global round is then $K(|\theta_0| + B \sum_{k=1}^K O_k)$.

Privacy: HFL algorithms typically share model updates or gradient information in messages. Gradients can potentially leak raw data information, as shown in previous work [48], [49]. However, in Flex-VFL, messages only contain embeddings and each party can only calculate the partial derivatives associated with the server model and its local model. Thus, gradient attacks proposed for HFL cannot be performed on Flex-VFL. Embeddings may be vulnerable to model inversion attacks [50], though these attacks can be mitigated by applying homomorphic encryption [44], [51] or secure multi-party computation [32] to Flex-VFL. As mentioned in Section III, we assume that all parties have access to the labels. There are many practical scenarios where data samples are private between the parties, but the labels are not, such as predicting credit score. However, if labels are private and only present at a single party, Flex-VFL can be augmented using the method proposed by Liu et al. [7], allowing gradient calculation without the need for sharing labels. The analysis in Section V still holds in this case.

V. ANALYSIS

In this section, we provide convergence analysis of Flex-VFL. To avoid cumbersome notation going forward, we define $\mathbf{g}_k^{r,t} := \mathbf{g}_k(\Phi_{-k}^r; \mathbf{h}_k(\theta_k^{r,t}; \mathbf{X}_k^B); \mathbf{y}^B)$ and drop Φ_{-k}^r from $\mathbf{D}_k(\cdot)$ when the context is clear.

We start by defining a recurrence relation for updates to the global model. Let G^r be the stack of gradient updates in a global round r :

$$\begin{aligned} \mathbf{G}^r &= \left[\sum_{t=0}^{\tau_0^r-1} \mathbf{D}_0(\theta_0^{r,0}, \dots, \theta_0^{r,t_0}), \dots, \sum_{t_K=0}^{\tau_K^r-1} \mathbf{D}_K(\theta_K^{r,0}, \dots, \theta_K^{r,t_K}) \right] \\ &= \left[\sum_{t=0}^{\tau_0^r-1} w_0^{r,t_0} \mathbf{g}_0^{r,t_0}, \dots, \sum_{t_K=0}^{\tau_K^r-1} w_K^{r,t_K} \mathbf{g}_K^{r,t_K} \right]. \end{aligned} \quad (9)$$

We can define our updates to the global model during a global round with the following recurrence relation:

$$\Theta^{r+1,0} = \Theta^{r,0} - \eta_k^r \mathbf{G}^r. \quad (10)$$

With the help of (10), we can model Flex-VFL as a gradient coordinate descent algorithm and analyze the algorithm convergence in this vein.

We note that each party reuses stale embeddings of the same mini-batch from other parties for multiple local iterations in Algorithm 1: each party k takes τ_k^r descent steps using mini-batch \mathcal{B}^r at a global round r . This indicates that the stochastic gradients are not unbiased during local iterations $t > 0$. However, using conditional expectation, we can apply

Assumption 2 to the gradient calculated at local iteration $t = 0$. If we take expectation over \mathcal{B}^r , conditioned on the previous models $\Theta^{\tau,0}$ up to round r , we obtain

$$\mathbb{E}_{\mathcal{B}^r}[\mathbf{g}_k^{r,0} \mid \{\Theta^{\tau,0}\}_{\tau=0}^r] = \nabla_m F(\Phi_{-k}^r; \mathbf{h}_k(\theta_k^{r,t})). \quad (11)$$

With the help of (11), we can prove convergence by bounding the difference between the gradient at the start of each global round and those calculated during local iterations.

In particular, we prove the following lemma:

Lemma 1. *If $\eta_k^r \leq \frac{1}{2\tau_k^r L_k \max_{0 \leq t \leq \tau_k^r-1} w_k^{r,t}}$, then under Assumptions 1–3 the weighted conditional expected squared norm difference of gradients $\mathbf{g}_k^{r,t}$ and $\mathbf{g}_k^{r,0}$ for a set of τ_k^r local iterations is bounded as follows:*

$$\begin{aligned} &\sum_{t=0}^{\tau_k^r-1} w_k^{r,t} \mathbb{E}^r \left[\left\| \mathbf{g}_k^{r,t} - \mathbf{g}_k^{r,0} \right\|^2 \right] \\ &\leq 8(\tau_k^r)^3 (\eta_k^r)^2 L_k^2 \max_{0 \leq t \leq \tau_k^r-1} (w_k^{r,t})^3 \left(\left\| \nabla_k F(\Theta^{r,0}) \right\|^2 + \sigma_k^2 \right) \end{aligned} \quad (12)$$

and

$$\begin{aligned} &\sum_{t=0}^{\tau_k^r-1} (w_k^{r,t})^2 \mathbb{E}^r \left[\left\| \mathbf{g}_k^{r,t} - \mathbf{g}_k^{r,0} \right\|^2 \right] \\ &\leq 8(\tau_k^r)^3 (\eta_k^r)^2 L_k^2 \max_{0 \leq t \leq \tau_k^r-1} (w_k^{r,t})^4 \left(\left\| \nabla_k F(\Theta^{r,0}) \right\|^2 + \sigma_k^2 \right) \end{aligned} \quad (13)$$

where \mathbb{E}^r is the expectation taken on the mini-batch \mathcal{B}^r conditioned on $\{\Theta^{\tau,0}\}_{\tau=0}^r$.

The proof of Lemma 1 can be found in Appendix B. Lemma 1 bounds the error incurred at each party in the stochastic partial derivatives during a set of local iterations as a result of using stale embeddings from other parties, as well as from using the same mini-batch for all local iterations in a single round. The lemma also captures the effect of different local optimizers at each party on the partial derivatives. Using Lemma 1, we can now analyze how this error accumulates over all iterations. Applying our smoothness assumption along with (10) and Lemma 1, we can prove that Flex-VFL converges.

We present our convergence result in the following theorem.

Theorem 1. *Under Assumptions 1–3, if η_k^r satisfies:*

$$\eta_k^r \leq \frac{1}{16\tau_k^r \max\{L, L_k\} \max_{0 \leq t \leq \tau_k^r-1} w_k^{r,t}} \quad (14)$$

then the weighted average squared gradient norm over all parties and R rounds of Algorithm 1 is bounded by:

$$\begin{aligned} &\frac{1}{S} \sum_{r=0}^{R-1} \sum_{k=0}^K \eta_k^r W_k^r \mathbb{E} \left[\left\| \nabla_k F(\Theta^{r,0}) \right\|^2 \right] \leq \frac{4}{S} (F(\Theta^{0,0}) - F^{\text{inf}}) \\ &+ \frac{4L}{S} \sum_{r=0}^{R-1} \sum_{k=0}^K (\eta_k^r)^2 W_k^r \max_{0 \leq t \leq \tau_k^r-1} w_k^{r,t} \tau_k^r \sigma_k^2 \end{aligned} \quad (15)$$

where F^{inf} is a lower bound on $F(\cdot)$, $S = \sum_{r=0}^{R-1} \sum_{k=0}^K \eta_k^r W_k^r$, and $W_k^r = \sum_{t=0}^{\tau_k^r-1} w_k^{r,t}$.

We provide the full proof of Theorem 1 in Appendix C.

The left-hand-side of (15) is a weighted average of all the partial derivatives' norms during the training. As this term approaches zero, Flex-VFL approaches a fixed point. The first term in the right-hand-side of (15) is similar to that of distributed gradient descent [45], and is affected by the difference in the initial and final models of the algorithm. The first term is the convergence rate term: as the number of global rounds R approaches ∞ , this first term goes to zero, while the second term, the additive convergence error, remains. The second term is the error associated with the variance in taking stochastic gradients steps, as well as the error incurred by running multiple local iterations.

If we let $\eta_k^r = \frac{1}{\sqrt{R \max_{k,r} \tau_k^r}}$ in (15), then we can see the convergence rate of Flex-VFL is $O(\frac{1}{\sqrt{R \max_{k,r} \tau_k^r}})$, the same as other VFL algorithms [7], [14], [16]. This indicates that we can achieve a fast convergence speed despite the error introduced by heterogeneous party speeds and local optimizers.

Effect of heterogeneous speeds: We observe that S appears in the denominator of the first term in (15); a larger value of S improves the convergence rate of Flex-VFL. This quantity S depends on the party learning rates η_k^r and the constraint (14) requires that η_k^r be inversely proportional to τ_k^r , the number of local iterations party k takes in round r . In addition, S increases with the sum of weights $w_k^{r,t}$ over τ_k^r local iterations. Consider the case where each party employs classical SGD, implying $w_k^{r,t} = 1$ for all parties over all iterations. In this case, $S = \sum_{r=0}^{R-1} \sum_{k=0}^K \eta_k^r \tau_k^r$. If we let $\eta_k^r = \frac{1}{\tau_k^r}$, then $S = R(K+1)$. If we instead consider a fixed learning rate $\eta_k^r = \eta$ across all parties and iterations, then to satisfy (14), $\eta = \frac{1}{\max_{k,r} \tau_k^r}$. In this case, $S = \sum_{r=0}^{R-1} \sum_{k=0}^K \frac{\tau_k^r}{\max_{k,r} \tau_k^r} \leq R(K+1)$. Thus, choosing the learning rates η_k^r according to each party's number of local iterations in a round τ_k^r can reduce the error in the first term of (15) and improve the convergence rate. However, τ_k^r may not always be known in advance. We discuss these findings further in Section VI, where we introduce Adaptive Flex-VFL.

Effect of heterogeneous optimizers: From Theorem 1, we can see that the first term in (15) decreases with larger local optimizer weights, while the second term increases with larger weights. Note that proper tuning of η_k^r for each party k can help offset the error introduced by $\max_{0 \leq t \leq \tau_k^r-1} w^t$ in the second term. We also note that the constraint (14) requires η_k^r to be inversely proportional $\max_{0 \leq t \leq \tau_k^r-1} w^t$. Thus there is tension between choosing larger optimizer weights and choosing a larger step size. In cases where η_k^r remains constant while still satisfying (14), Theorem 1 indicates that weights larger than 1, such as when using momentum and proximal steps, can improve the convergence rate by decreasing the first term in (15). However, it can also negatively affect the error as $R \rightarrow \infty$ by increasing the second term in (15). If all else is constant, a large W_k^r is beneficial when σ_k is small. In other words, in cases where stochastic variance is small, our analysis shows a potential benefit for using local optimizers other than classical SGD.

We now introduce some corollaries to study the convergence rate of Flex-VFL. We first consider the case where each party

has the same stochastic variance, runs the same number of local iterations, and uses SGD locally.

Corollary 1. Suppose $\sigma_k = \sigma$, $\tau_k^r = \tau$, and $\eta_k^r = \eta$ for all parties k and rounds r . Let $w_k^{r,t} = 1$ for all rounds r , local iterations t , and parties k . Under Assumptions 1-3, if η satisfies:

$$\eta \leq \frac{1}{16\tau \max\{L, L_k\}} \quad (16)$$

then the average squared gradient norm over all parties and R rounds of Algorithm 1 is bounded by:

$$\frac{1}{R} \sum_{r=0}^{R-1} \mathbb{E} [\|\nabla F(\Theta^{r,0})\|^2] \leq \frac{4(F(\Theta^{0,0}) - F^{\text{inf}})}{R\eta\tau(K+1)} + 4L\eta\tau\sigma^2 \quad (17)$$

If we let $\eta = \frac{1}{\sqrt{\tau R}}$ in Corollary 1, then we can see our convergence rate is $O(\frac{1}{\sqrt{\tau R}})$, which is the same as distributed SGD algorithms [9], [45], [52].

We consider a decaying learning rate in the following corollary.

Corollary 2. Suppose $\eta_k^r \leq \frac{1}{16\tau_k^r \max\{L, L_k\} \max_{0 \leq t \leq \tau_k^r-1} w_k^{r,t}}$, and suppose that $\sum_{r=0}^{\infty} \eta_k^r = \infty$ and $\sum_{r=0}^{\infty} (\eta_k^r)^2 < \infty$ for all parties k . Then under Assumptions 1-3, the left-hand-side of (15) goes to zero as R approaches ∞ .

Corollary 2 states that given a sequence of learning rates that are not summable, but square summable, then Algorithm 1 achieves convergence to a fixed point. One possible choice for learning rates to satisfy these conditions is by diminishing η_k^r at a rate of $O(\frac{1}{r})$ where r is the current global round. This is a standard step size requirement of SGD algorithms for non-convex objectives [45].

VI. ADAPTIVE EXTENSION

In this section, we present an adaptive extension to Flex-VFL, which we call Adaptive Flex-VFL. One can think of Adaptive Flex-VFL as a meta-optimization algorithm where the server keeps track of party operating speeds and local optimizer parameters during each global round in order to choose the best learning rates for convergence speed.

Let $\bar{w}_k^r := \max_{0 \leq t \leq \tau_k^r-1} w_k^{r,t}$. According to Theorem 1, the learning rate η_k^r at a given global round r for party k must be inversely proportional to the number of local iterations τ_k^r and the largest weight applied during local iterations \bar{w}_k^r . We also know that the first term of (15) is the main contributor to the convergence rate in Flex-VFL, while the second term is the convergence floor, mostly affected by the stochastic variance. If the bound (14) on the learning rates η_k^r holds, the second term's effect is minimal. Therefore, based on our analysis, a natural improvement to Flex-VFL is to maximize η_k^r subject to (14) in each global round, tailoring each party's learning rate to their specific operating rate and local optimizer parameters.

Adaptive Flex-VFL is outlined in Algorithm 2. For the first global round, τ_k^0 for each party is estimated, either with prior knowledge of the party operating speeds, or by running a dummy global round. Each party can communicate \bar{w}_k^0 to the

Algorithm 2 Adaptive Flexible Vertical Federated Learning

```

1: Initialize:  $\theta_k^{1,0}$  for all parties  $k$  and server model  $\theta_0^{1,0}$ 
2: Initialize:  $A_k$  and  $\eta_k^1 = \frac{A_k}{\tau_k^0 \bar{w}_k^0}$  for all parties
3: for  $r \leftarrow 1, \dots, R$  do
4:   Sample a mini-batch  $\mathcal{B}^r \in \{\mathbf{X}, \mathbf{y}\}$ 
5:   for  $k \leftarrow 1, \dots, K$  in parallel do
6:     Sample features  $\mathbf{X}_k^{\mathcal{B}^r}$  corresponding to IDs in  $\mathcal{B}^r$ 
7:     Send  $\mathbf{h}_k(\theta_k^{r,0}; \mathbf{X}_k^{\mathcal{B}^r})$  to server
8:   end for
9:    $\Phi^r \leftarrow \{\theta_0^{r,0}, \mathbf{h}_1(\theta_1^{r,0}), \dots, \mathbf{h}_K(\theta_K^{r,0})\}$ 
10:  Server sends  $\Phi^r$  to all parties
11:  for  $k \leftarrow 0, \dots, K$  in parallel do
12:    for  $t \leftarrow 0, \dots, \tau_k^r - 1$  do
13:       $\theta_k^{r,t+1} \leftarrow \theta_k^{r,t} - \eta_k^r \mathbf{D}_k(\Phi_{-k}^r; \mathbf{h}_k(\theta_k^{r,t}); \mathbf{y}^{\mathcal{B}})$ 
14:    end for
15:    Send  $\tau_k^r$  and  $\bar{w}_k^r$  to server
16:  end for
17:  Server sets  $\eta_k^{r+1} \leftarrow \frac{A_k}{\tau_k^r \bar{w}_k^r}$  for all parties
18: end for

```

server before the start of training. All η_k^1 are initialized to some $\frac{A_k}{\tau_k^0 \bar{w}_k^0}$, where A_k is chosen small enough to satisfy (14). At the end of each global round, the server gathers information about how many local iterations each party took, τ_k^r , and their maximum weight applied to gradients during local iterations, \bar{w}_k^r . We let $\eta_k^{r+1} = \frac{A_k}{\tau_k^r \bar{w}_k^r}$. If we assume that for each party k , τ_k^r and $w_k^{r,t}$ do not change too rapidly across global rounds, the server can accurately estimate the appropriate learning rate to assign to each party that will maximize the convergence rate.

We now define more formal conditions under which Adaptive Flex-VFL is guaranteed to converge according to Theorem 1. Suppose the maximum rate of change of $\tau_k^r \bar{w}_k^r$ from a round r to $r+1$ is α :

$$\frac{\tau^r \bar{w}_k^r}{\tau^{r+1} \bar{w}_k^{r+1}} \leq \alpha. \quad (18)$$

Note that $\eta_k^{r+1} = \frac{A_k}{\tau^r \bar{w}_k^r}$. In order to satisfy constraint (14), we need $\eta_k^{r+1} \leq \frac{1}{16 \max\{L, L_k\} \tau^{r+1} \bar{w}_k^{r+1}}$. Therefore, we need A_k to be chosen such that:

$$\frac{A_k}{\tau^r \bar{w}_k^r} \leq \frac{1}{16 \max\{L, L_k\} \tau^{r+1} \bar{w}_k^{r+1}} \quad (19)$$

$$A_k \leq \alpha \left(\frac{1}{16 \max\{L, L_k\}} \right). \quad (20)$$

Thus, in order for Adaptive Flex-VFL to satisfy (14) in all rounds of training, A_k must satisfy (20). We note that in practice, as we show in Section VII, Adaptive Flex-VFL can show a clear improvement over Flex-VFL with a fixed learning rate.

VII. EXPERIMENTS

Next, we present experiments to compare Flex-VFL with synchronous and asynchronous VFL algorithms, and to observe the effect of the adaptive extension to Flex-VFL in practice.¹

¹Code for experiments available at <https://github.com/rpi-nsf/flex-vfl>

A. Datasets and Experimental Setup

We utilize three datasets for our experiments: the MOSEI dataset [53], the ImageNet dataset [54], and the ModelNet40 dataset [55]. For each dataset and VFL algorithm, we performed a grid search to choose the best learning rate and regularization parameters (where applicable); we trained each algorithm with different hyperparameters for 100 epochs and chose the hyperparameters with the lowest training loss.

MOSEI: CMU-MOSEI is a multimodal dataset for sentiment analysis. The dataset consists of 23,453 sentences from YouTube videos giving opinions on various topics. The dataset includes video, audio, and text data, and each sentence is labeled with sentiment values, scoring the positivity or negativity of the sentence. For our experimental setup, we consider a case with three parties, where each party stores one type of data. The parties with video and audio train local LSTMs, and the party with text trains a BERT model. The server model consists of a three-layer fully-connected neural network. We use an L1 loss function with L2 regularization. The parties train using SGD with a batch size of 50. For the video and audio parties the learning rate was selected from $\{0.01, 0.005, 0.001, 0.0005\}$. For the text party the learning rate was selected from $\{5 \times 10^{-5}, 1 \times 10^{-5}, 5 \times 10^{-6}\}$. The regularization coefficient was selected from $\{0, 10^{-3}, 10^{-4}, 10^{-5}\}$.

ImageNet100: The ImageNet dataset consists of images from several classes of objects. In our experiments, we randomly choose 100 classes from the ImageNet dataset (ImageNet100), consisting of $\sim 130,000$ images. We consider a case with 4 parties, each storing a quadrant of each image. Each party trains ResNet50 locally and the server trains a single fully connected layer. We use a cross-entropy loss function with L2 regularization. The parties train using a batch size of 256. Each party trains using SGD with local momentum with $\rho = 0.9$. The initial learning rate for each party was selected from $\{0.3, 0.08, 0.03, 0.008, 0.003\}$ and the regularization coefficient was selected from $\{0, 10^{-3}, 10^{-4}, 10^{-5}\}$. The learning rate decays by a factor of 10 every $\sim 75,000$ local iterations.

ModelNet40: The ModelNet40 dataset are images of CAD models with 40 classes of objects, each with 12 different camera views. In our experiments, we consider a setup with 12 parties, each with a single view of each CAD model. Each party trains ResNet50 locally and the server trains a single fully connected layer. We use a cross-entropy loss function for training. The parties train using a batch size of 64. Each party trains using SGD with local momentum with $\rho = 0.9$. The learning rate for each party was selected from $\{1 \times 10^{-3}, 5 \times 10^{-4}, 1 \times 10^{-4}, 5 \times 10^{-5}\}$.

Baselines: We compare Flex-VFL with synchronous and asynchronous VFL methods. We limit our comparisons to those that support arbitrary party feature extractors and arbitrary server fusion networks, as well as multiple local iterations [7], [8], [14].

- **Sync-VFL** Synchronous VFL is a special case of Flex-VFL where all parties run the same number of local iterations, regardless of party operating speeds. When parties all use standard SGD and the server model has no trainable parameters, Sync-VFL is equivalent to the VFL algorithm

TABLE II: Time to reach target mean-squared error (MAE) on the MOSEI using different optimizer combinations. The value shown is the mean of 5 runs, \pm the standard deviation.

Video/Audio Optimizers	Text Optimizer	Time units ($\times 10^3$) to reach target
SGD	SGD	64.55 ± 11.74
Local Momentum	SGD	35.21 ± 11.74
SGD	Local Momentum	29.34 ± 0.00
Local Momentum	Local Momentum	41.08 ± 14.37

proposed by Liu et al [7]. For our experiments, we consider two cases of Sync-VFL: Sync-Min-VFL and Sync-Max-VFL.

- **Sync-Min-VFL:** Flex-VFL and Sync-VFL use the same choice of local training timeout, meaning each party in Sync-VFL runs $\tau^r = \min_k \tau_k^r$ descent steps before synchronizing.
- **Sync-Max-VFL:** Sync-VFL waits for all parties to run $\tau^r = \max_k \tau_k^r$ descent steps before synchronizing. This means that Sync-Max-VFL ensures that all parties run the same number of iterations as the fastest party in Flex-VFL, which extends the duration of a global round to accommodate the slowest party.
- **VAFL:** In VAFL [14], each party calculates its embeddings for a randomly selected mini-batch. The party then immediately exchanges information with the server to update both the server model and party’s model parameters. Parties may take different lengths of time to execute their individual training steps, and so the model updates are asynchronous.
- **P-BCD:** We also include a baseline for Flex-VFL where we set $\tau_k^r = 1$ for all k and r . This is equivalent to parallel block coordinate descent (P-BCD) [56].

Time units: In each of our experiments, we measure time-to-target in terms of simulated time units. We define the communication time with the server, the computation time for each party, and the local training timeout to be used by Flex-VFL and Sync-VFL in terms of these time units. The time units taken to complete a local iteration and the timeout chosen inform how many local iterations each party will perform in Flex-VFL and Sync-VFL. For example, suppose two parties take 5 and 10 time units to complete a local iteration, respectively, and the timeout is set to 20. In Sync-VFL, both parties will complete two local iterations. In Flex-VFL, the first party will complete four local iterations while the second party completes two.

B. Heterogeneous Optimizers

We first study the effect of training with heterogeneous optimizers. We run Flex-VFL and train on the MOSEI dataset with parties either using standard SGD or SGD with local momentum. We consider a case where all parties and the server have the same operating rate. We let the computation time for each party be 1 time unit and set the timeout for each global round to be 20 time units. Thus, each party runs 20 local iterations in each global round. We let the communication latency be 10 time units. We measure the average time taken to achieve a target mean-square error (MAE) over 5 runs. The results are given in Table II. The best optimizer combination

over the five runs is using standard SGD at the video and audio parties that train LSTMs, while the text party uses SGD with local momentum to train the BERT model. Thus we can see a benefit from choosing different optimizers at each party depending on the local model architecture. We use this combination of optimizers for the rest of the experiments with the MOSEI dataset.

C. Fixed Operating Speeds

We next study the setting where party operating speeds are heterogeneous but remain fixed throughout training. For each dataset we define the speed of a party by how many time units it takes for it to complete a local iteration, as well as a local training timeout to be used by Flex-VFL and Sync-VFL.

For MOSEI, we set the timeout to 20 time units, and set the operating rates such that the parties storing video, audio, and text take 5, 10, and 15 local iterations before the timeout, respectively, while the server completes 20 local iterations before the timeout. For ImageNet100, we set the timeout to 10 time units, and set the operating rates such that the four parties take 2, 4, 6, and 8 local iterations before the timeout, respectively, while the server completes 10 local iterations. For ModelNet40, we set the timeout to 20 time units, set the operating rates such that server take 20 local iterations before the timeout, and let groups of 3 parties each take 5, 10, 15, and 20 local iterations, respectively. These operating rates are chosen such that there are an equal number of stragglers, medium speed parties, and fast parties in the system.

We simulate three communication network settings, representing cases of different ratios of computation time versus communication time. We denote the round-trip message latency with the server as t_{comm} and we let the time for the fastest party to complete a local iteration be 1 time unit. In the first setting, we assume communication latency with the server is very low, equal to computation time of a single local iteration, and let $t_{\text{comm}} = 1$ unit. In the second setting, we consider a case where communication time starts to outweigh computation time of a single local iteration, and set $t_{\text{comm}} = 10$ units. In this case, communication with the server takes 10 local iterations at the fastest party. For the final setting, we consider the case where there is very high communication latency, setting $t_{\text{comm}} = 50$ units. Such high communication latency can occur when parties are globally distributed.

In Table III we show the time units it takes to reach a target test accuracy. For the MOSEI dataset, we let the target be 0.65 Mean Absolute Error (MAE), a common measure of performance for the dataset. We can see that for the MOSEI dataset, P-BCD and VAFL perform best when communication latency is low. However, as communication latency increases, Flex-VFL is able to reach the target MAE twice as fast as Sync-Min-VFL and P-BCD, and four times as fast as VAFL. For the ImageNet100 dataset, the target is set to 60% top-5 accuracy. In this case, P-BCD performs well when communication latency is low. As the communication latency increases however, Flex-VFL overtakes P-BCD, benefiting from local iterations saving on overall communication. Finally, for the ModelNet40 dataset, the target is set to 70%. Here, Flex-VFL always performs

TABLE III: Time units taken to reach target test accuracy under different communication times. For the MOSEI dataset, the target is reaching 0.65 MAE. For ImageNet100, target is reaching 60% top-5 accuracy. For ModelNet40, the target is reaching 70% top-5 accuracy. The value shown is the mean of 5 runs, \pm the standard deviation. A “—” indicates that the target was not reached during training.

Comm. Time	Algorithm	Time units ($\times 10^3$) to reach target		
		MOSEI Target=0.65 MAE	ImageNet100 Target=60% Top-5 Acc.	ModelNet40 Target=70% Top-5 Acc.
1 unit	P-BCD	5.22 \pm 0.65	73.06 \pm 2.38	44.51 \pm 0.90
	VAFL	7.63 \pm 1.12	89.59 \pm 8.67	52.27 \pm 2.17
	Sync-Min-VFL	13.69 \pm 0.00	299.48 \pm 19.17	32.34 \pm 2.05
	Sync-Max-VFL	26.41 \pm 0.00	520.05 \pm 63.06	84.82 \pm 4.99
	Flex-VFL	6.85 \pm 0.00	113.26 \pm 31.07	25.23 \pm 2.42
10 units	P-BCD	14.60 \pm 1.83	182.66 \pm 5.94	124.62 \pm 2.51
	VAFL	29.60 \pm 3.18	—	161.02 \pm 3.93
	Sync-Min-VFL	19.56 \pm 0.00	544.50 \pm 34.86	46.20 \pm 2.92
	Sync-Max-VFL	29.34 \pm 0.00	611.82 \pm 74.19	94.25 \pm 5.54
	Flex-VFL	9.78 \pm 0.00	205.92 \pm 56.49	36.04 \pm 3.46
50 units	P-BCD	56.33 \pm 7.04	669.74 \pm 21.78	480.66 \pm 9.70
	VAFL	96.09 \pm 6.41	—	—
	Sync-Min-VFL	45.64 \pm 0.00	1633.50 \pm 104.58	107.80 \pm 6.82
	Sync-Max-VFL	42.38 \pm 0.00	1019.70 \pm 123.65	136.14 \pm 8.01
	Flex-VFL	22.82 \pm 0.00	617.76 \pm 169.47	84.08 \pm 8.07

better than the other algorithms, regardless of communication latency. In our experiments with ModelNet40, there are a larger number of parties than in the other datasets. This causes the heterogeneity of party operating speeds to have a greater effect on time-to-target accuracy. With the chosen distribution of party operating speeds, Flex-VFL reaches a target accuracy up to four times as fast than other VFL algorithms. In the next subsection, we consider how different operating speed distributions can affect performance of each VFL algorithm.

D. Uniform Versus Average Operating Rates

For our next experiment, we again consider fixed operating speeds, and now focus on the effect of operating rate distribution. Specifically, we compare an evenly distributed case of party operating speeds to a typical case, and show how Flex-VFL, Sync-VFL, VAFL, and P-BCD perform. For these experiments, we use the ModelNet40 dataset, and consider two distributions of party operating speeds. For Flex-VFL and Sync-VFL, we use a local training timeout of 20 time units. The first distribution is the same as the previous experiment: the timeout is set to 20 time units, and the operating rates are set such that the server takes 20 local iterations per round, and groups of 3 parties each take 5, 10, 15, and 20 local iterations, respectively. For determining a realistic typical case of party operating speeds, we use Google’s Cluster Data [57], a dataset of workload traces running on Google compute cells. We choose 13 random traces from the dataset, and take the average CPU usage for each to determine the operating speed of parties for these experiments. For a party k , we let the time to complete a local iteration be $(1 - c_k)^{-1}$ for all r rounds, where c_k is the k -th machine’s average CPU utilization. Since the timeout is 20 time units, $\tau_k^r = 20 \cdot (1 - c_k)$ for all r rounds.

In Figure 2 we present the results of training with the different operating rate distributions. We plot the top-5 test accuracy against time units. In Figures 2a and 2b, we see the results when party operating speeds are evenly distributed. In this case, we can see that when communication time is low, Flex-VFL and VAFL perform well, as they are robust to the stragglers in the system. P-BCD also performs well here. We

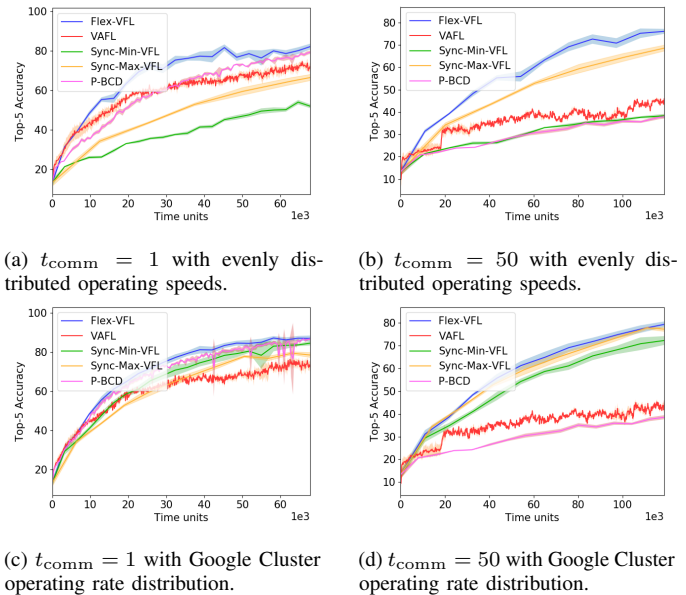


Fig. 2: Top-5 test accuracy plotted against time units for ModelNet40 dataset with uniform and average distribution of party operating speeds. The solid lines are the mean of 5 runs, while the shaded region represents the standard deviation.

believe this is because P-BCD does not incur error introduced by local iterations. When communication latency is high though, we can see that Flex-VFL continues to perform well while VAFL and P-BCD start to perform worse. In Figures 2c and 2d, we see the results for operating speeds using the Google Cluster data. In this case, we can see that Flex-VFL performs the same or better than Sync-Min-VFL and P-BCD when communication latency is low. When communication latency is high, Flex-VFL performs the same or better than Sync-Max-VFL. Flex-VFL in these cases is always the best choice of algorithm regardless of party operating rate distributions or communication time.

E. Effect of Local Training Timeout

In this section, we explore the effect of different timeouts with fixed operating rates on the time-to-target accuracy of Flex-VFL. For these experiments, we use the ModelNet40 dataset and use the even distribution of operating rates from previous experiments. We let the communication time be 10 time units. We also include results from Sync-Max-VFL as a baseline. Recall that Sync-Max-VFL ensures all parties to run the same number of local iterations as the fastest party does in Flex-VFL. For example, if the fastest party in Flex-VFL runs 20 local iterations, then all parties in Sync-Max-VFL run 20 local iterations.

Table IV shows the time taken for Sync-VFL and Flex-VFL to achieve 70% top-5 accuracy on the ModelNet40 dataset for different timeouts. We see that for Flex-VFL, increasing the timeout improves the time-to-target, up until a timeout of 40 time units. We see this same trend with Sync-VFL when changing the number of local iterations. This is in line with previous works that explore the effect of local iterations on convergence rate [3], [7], [58]. Increasing the number of local iterations improves time-to-target up to a certain point, where

TABLE IV: Time units taken to reach 70% top-5 test accuracy on the ModelNet40 dataset. On the left, we include the time-to-target accuracy for Flex-VFL for timeouts of 20 to 40 units. On the right, we include the time-target accuracy of Sync-VFL for 20 to 40 local iterations. For example, in row 1, the fastest party in Flex-VFL runs 20 local iterations, while all parties in Sync-VFL run 20 local iterations. Communication time is 10 units. The value shown is the mean of 5 runs, \pm the standard deviation.

Local Training Period Timeout	Flex-VFL	Local Iterations Per Round	Sync-VFL
	Time units ($\times 10^3$) to reach target		Time units ($\times 10^3$) to reach target
20 units	36.04 \pm 3.46	20 iterations	94.25 \pm 5.54
25 units	30.49 \pm 3.70	25 iterations	72.07 \pm 5.54
30 units	24.02 \pm 1.85	30 iterations	60.98 \pm 6.79
35 units	22.18 \pm 1.85	35 iterations	58.21 \pm 5.54
40 units	33.26 \pm 1.85	40 iterations	85.93 \pm 5.54

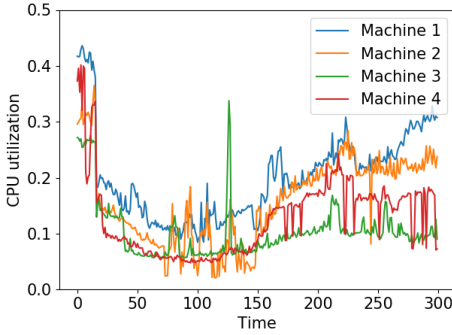


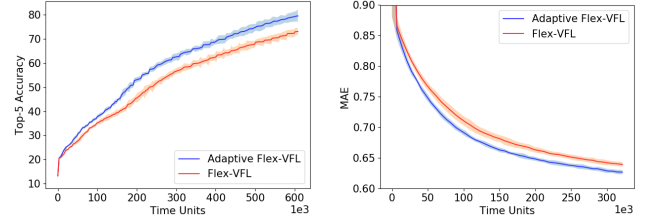
Fig. 3: CPU utilization over time of 4 machines from the Google Cluster workload dataset.

the error incurred by local iterations outweighs the benefits to convergence rate. We can also see in Table IV that Flex-VFL outperforms Sync-VFL regardless of the timeout.

F. Variable Operating Speeds

We next investigate the setting where party operating speeds change during training. To model realistic changes in these rates, we again use Google’s Cluster Data [57]. In Figure 3, we plot the CPU utilization of 4 randomly chosen machine traces over a short time interval. For a party k , we let the time to complete a local iteration be $(1 - c_k^r)^{-1}$ where c_k^r is the k -th machine’s CPU utilization at global round r . We set $\tau_k^r = t_o \cdot (1 - c_k^r)$ for round r , where t_o is the local training timeout.

We compare Flex-VFL and Adaptive Flex-VFL, and train on the ModelNet40 and MOSEI datasets. For ModelNet40, we use a timeout of 10 time units and set $A_k = 0.0001$, and for MOSEI, we use a timeout of 20 time units and set $A_k = 5 \times 10^{-5}$ for the text party and $A_k = 0.001$ for the other parties and server. In both cases, we let the communication time be 1 time unit. For static Flex-VFL, the server chooses $\eta_k = \eta_k^r$ such that (14) is not violated at any point during training. This is determined using the largest value τ_k^r over all rounds r , which is 10 for ModelNet40 and 20 for MOSEI, corresponding to the case when the CPU utilization is $c_k^r = 0$. Adaptive Flex-VFL, on the other hand, chooses η_k^r in each



(a) ModelNet40 dataset

(b) MOSEI dataset

Fig. 4: Top-5 test accuracy and test mean absolute error (MAE) of adaptive and static methods of Flex-VFL training on the ModelNet40 and MOSEI datasets respectively.

global round based on the previous rounds values of τ_k^r and $\max_{0 \leq t \leq \tau_k^r - 1} w_k^{r,t}$, as described in Algorithm 2.

In Figures 4a and 4b, we show the top-5 test accuracy of training on the ModelNet40 and MOSEI datasets, respectively. We can see that Adaptive Flex-VFL reaches a much higher test accuracy and lower MAE in a shorter period of training than Flex-VFL. In ModelNet40, Adaptive Flex-VFL reaches a top-5 accuracy of 70% about 130 time units faster than Flex-VFL. In MOSEI, Adaptive Flex-VFL achieves an MAE of 0.65 about 70 time units faster than Flex-VFL. Allowing the learning rates to increase when CPU utilization is lower can greatly improve the convergence rate of Flex-VFL.

VIII. CONCLUSION

We proposed Flex-VFL, a vertical federated learning algorithm that learns on distributed, vertically-partitioned data in a system with heterogeneous parties. We analyzed Flex-VFL and showed the benefit of optimizers that utilize momentum or proximal steps in VFL settings. We also showed that convergence requires that each party’s learning rate is tailored to its operating speed and local optimizer. Based on this observation, we proposed Adaptive Flex-VFL, which optimizes party learning rates at each global round based on party operating speeds and optimizer parameters. In our experiments, we demonstrated that Flex-VFL can outperform both synchronous and asynchronous VFL algorithms, reaching a target accuracy up to $4\times$ faster than other VFL algorithms. Our experiments also indicate that Flex-VFL is often the best overall choice of VFL algorithms when it’s necessary to be flexible with high communication latency and different party operating rate distribution. We also provided experimental results comparing Adaptive Flex-VFL and Flex-VFL using real-world party operating speeds. We found that Adaptive Flex-VFL can improve time-to-target accuracy by 30% over Flex-VFL. In future work, we will explore the impact of partial participation of VFL parties on algorithm performance.

ACKNOWLEDGMENT

This material is based upon work supported in part by the National Science Foundation under Grant CNS-1553340, and by the Rensselaer-IBM AI Research Collaboration (<http://airc.rpi.edu>), part of the IBM AI Horizons Network.

APPENDIX

In this section, we provide our full proof of Theorem 1. We start by introducing some additional notation and providing the proof of Lemma 1.

A. Additional Notation

We define

$$\gamma_{k,j}^{r,t} = \begin{cases} \theta_j^{r,t} & k = j \\ \theta_j^{r,0} & \text{otherwise} \end{cases} \quad (21)$$

to represent party k 's view of party j 's model in round r and iteration t . We define the column vector $\Gamma_k^{r,t} = [\gamma_{k,0}^{r,t}; \dots; \gamma_{k,K}^{r,t}]$ to be party k 's view of the system model in round r and iteration t .

B. Proof of Lemma 1

We now prove Lemma 1, stated in Section V.

Proof. We start by bounding the expected squared norm difference between gradients at the start of the global round r and local iteration t :

$$\begin{aligned} & \mathbb{E}^r \left[\left\| \mathbf{g}_k^{r,t} - \mathbf{g}_k^{r,0} \right\|^2 \right] \\ &= \mathbb{E}^r \left[\left\| \mathbf{g}_k^{r,t} - \mathbf{g}_k^{r,t-1} + \mathbf{g}_k^{r,t-1} - \mathbf{g}_k^{r,0} \right\|^2 \right] \end{aligned} \quad (22)$$

$$\begin{aligned} & \leq (1+n) \mathbb{E}^r \left[\left\| \mathbf{g}_k^{r,t} - \mathbf{g}_k^{r,t-1} \right\|^2 \right] \\ & \quad + \left(1 + \frac{1}{n} \right) \mathbb{E}^r \left[\left\| \mathbf{g}_k^{r,t-1} - \mathbf{g}_k^{r,0} \right\|^2 \right] \end{aligned} \quad (23)$$

where (23) follows from the fact that $(X+Y)^2 \leq (1+n)X^2 + (1+\frac{1}{n})Y^2$ for some positive n .

Applying Assumption 1 to the first term in (23) we have:

$$\begin{aligned} & \mathbb{E}^r \left[\left\| \mathbf{g}_k^{r,t} - \mathbf{g}_k^{r,0} \right\|^2 \right] \\ & \leq (1+n) L_k^2 \mathbb{E}^r \left[\left\| \Gamma_k^{r,t} - \Gamma_k^{r,t-1} \right\|^2 \right] \\ & \quad + \left(1 + \frac{1}{n} \right) \mathbb{E}^r \left[\left\| \mathbf{g}_k^{r,t-1} - \mathbf{g}_k^{r,0} \right\|^2 \right] \quad (24) \\ & = (1+n) (\eta_k^r)^2 L_k^2 (w_k^{r,t-1})^2 \mathbb{E}^r \left[\left\| \mathbf{g}_k^{r,t-1} \right\|^2 \right] \\ & \quad + \left(1 + \frac{1}{n} \right) \mathbb{E}^r \left[\left\| \mathbf{g}_k^{r,t-1} - \mathbf{g}_k^{r,0} \right\|^2 \right] \end{aligned} \quad (25)$$

where (25) follows from the update rule $\theta_k^{r,t} = \theta_k^{r,t-1} - \eta_k^r w_k^{r,t-1} \mathbf{g}_k^{r,t-1}$.

We now add and subtract $\mathbf{g}_k^{r,0}$ to the first term in (25):

$$\begin{aligned} & \mathbb{E}^r \left[\left\| \mathbf{g}_k^{r,t} - \mathbf{g}_k^{r,0} \right\|^2 \right] \\ & \leq (1+n) (\eta_k^r)^2 L_k^2 (w_k^{r,t-1})^2 \mathbb{E}^r \left[\left\| \mathbf{g}_k^{r,t-1} - \mathbf{g}_k^{r,0} + \mathbf{g}_k^{r,0} \right\|^2 \right] \\ & \quad + \left(1 + \frac{1}{n} \right) \mathbb{E}^r \left[\left\| \mathbf{g}_k^{r,t-1} - \mathbf{g}_k^{r,0} \right\|^2 \right] \end{aligned} \quad (26)$$

$$\begin{aligned} & \leq 2(1+n) (\eta_k^r)^2 L_k^2 (w_k^{r,t-1})^2 \mathbb{E}^r \left[\left\| \mathbf{g}_k^{r,t-1} - \mathbf{g}_k^{r,0} \right\|^2 \right] \\ & \quad + 2(1+n) (\eta_k^r)^2 L_k^2 (w_k^{r,t-1})^2 \mathbb{E}^r \left[\left\| \mathbf{g}_k^{r,0} \right\|^2 \right] \\ & \quad + \left(1 + \frac{1}{n} \right) \mathbb{E}^r \left[\left\| \mathbf{g}_k^{r,t-1} - \mathbf{g}_k^{r,0} \right\|^2 \right]. \end{aligned} \quad (27)$$

If we let $n = \tau_k^r$, we can bound (27) further:

$$\begin{aligned} & \mathbb{E}^r \left[\left\| \mathbf{g}_k^{r,t} - \mathbf{g}_k^{r,0} \right\|^2 \right] \\ & \leq 2(1+\tau_k^r) (\eta_k^r)^2 L_k^2 (w_k^{r,t-1})^2 \mathbb{E}^r \left[\left\| \mathbf{g}_k^{r,t-1} - \mathbf{g}_k^{r,0} \right\|^2 \right] \\ & \quad + 2(1+\tau_k^r) (\eta_k^r)^2 L_k^2 (w_k^{r,t-1})^2 \mathbb{E}^r \left[\left\| \mathbf{g}_k^{r,0} \right\|^2 \right] \\ & \quad + \left(1 + \frac{1}{\tau_k^r} \right) \mathbb{E}^r \left[\left\| \mathbf{g}_k^{r,t-1} - \mathbf{g}_k^{r,0} \right\|^2 \right]. \end{aligned} \quad (28)$$

Let $\eta_k^r \leq \frac{1}{2\tau_k^r L_k \max_{0 \leq t \leq \tau_k^r-1} w_k^{r,t}}$. We bound (28) as follows:

$$\begin{aligned} & \mathbb{E}^r \left[\left\| \mathbf{g}_k^{r,t} - \mathbf{g}_k^{r,0} \right\|^2 \right] \\ & \leq \left(1 + \frac{2}{\tau_k^r} \right) \mathbb{E}^r \left[\left\| \mathbf{g}_k^{r,t-1} - \mathbf{g}_k^{r,0} \right\|^2 \right] \\ & \quad + 2(1+\tau_k^r) (\eta_k^r)^2 L_k^2 \max_{0 \leq t \leq \tau_k^r-1} (w_k^{r,t})^2 \mathbb{E}^r \left[\left\| \mathbf{g}_k^{r,0} \right\|^2 \right]. \end{aligned} \quad (29)$$

We define the following notation for simplicity:

$$A^{r,t} := \mathbb{E}^r \left[\left\| \mathbf{g}_k^{r,t} - \mathbf{g}_k^{r,0} \right\|^2 \right] \quad (30)$$

$$B := 2(1+\tau_k^r) (\eta_k^r)^2 L_k^2 \max_{0 \leq t \leq \tau_k^r-1} (w_k^{r,t})^2 \mathbb{E}^r \left[\left\| \mathbf{g}_k^{r,0} \right\|^2 \right] \quad (31)$$

$$C := \left(1 + \frac{2}{\tau_k^r} \right). \quad (32)$$

Note that we have shown that $A^{r,t} \leq C A^{r,t-1} + B$. Utilizing this bound, we can also show that:

$$A^{r,1} \leq C A^{r,0} + B \quad (33)$$

$$A^{r,2} \leq C^2 A^{r,0} + C B + B \quad (34)$$

$$A^{r,3} \leq C^3 A^{r,0} + C^2 B + C B + B \quad (35)$$

\vdots

$$A^{r,t} \leq C^t A^{r,0} + B \sum_{\tau_1=0}^{t-1} C^{\tau_1}. \quad (36)$$

Note that $A^{r,0} = \mathbb{E}^r \left[\left\| \mathbf{g}_k^{r,0} - \mathbf{g}_k^{r,0} \right\|^2 \right] = 0$. It is left to bound the second term in (36) over the set of local iterations.

$$\begin{aligned} & \sum_{t=0}^{\tau_k^r-1} w_k^{r,t} B \sum_{\tau_1=0}^{t-1} C^{\tau_1} \\ & = B \sum_{t=0}^{\tau_k^r-1} w_k^{r,t} \left(\frac{C^t - 1}{C - 1} \right) \end{aligned} \quad (37)$$

$$= \frac{B}{C-1} \sum_{t=0}^{\tau_k^r-1} w_k^{r,t} (C^t - 1) \quad (38)$$

$$= \frac{B}{C-1} \max_{0 \leq t \leq \tau_k^r-1} w_k^{r,t} \left(\frac{C^{\tau_k^r} - 1}{C-1} - \tau_k^r \right) \quad (39)$$

$$= \frac{B}{C-1} \max_{0 \leq t \leq \tau_k^r-1} w_k^{r,t} \left(\frac{\left(1 + \frac{2}{\tau_k^r}\right)^{\tau_k^r} - 1}{\frac{2}{\tau_k^r}} - \tau_k^r \right) \quad (40)$$

$$\leq \frac{(\tau_k^r)^2 B}{2} \max_{0 \leq t \leq \tau_k^r-1} w_k^{r,t} \left(\frac{e^2 - 1}{2} - 1 \right) \quad (41)$$

$$\leq 2(\tau_k^r)^2 B \max_{0 \leq t \leq \tau_k^r-1} w_k^{r,t}. \quad (42)$$

Plugging the definition of B into (42):

$$\begin{aligned} & \sum_{t=0}^{\tau_k^r-1} w_k^{r,t} B \sum_{\tau_1=0}^{t-1} C^{\tau_1} \\ & \leq 4(\tau_k^r)^2 (1 + \tau_k^r) (\eta_k^r)^2 L_k^2 \max_{0 \leq t \leq \tau_k^r-1} (w_k^{r,t})^3 \mathbb{E}^r \left[\left\| \mathbf{g}_k^{r,0} \right\|^2 \right] \end{aligned} \quad (43)$$

$$\leq 8(\tau_k^r)^3 (\eta_k^r)^2 L_k^2 \max_{0 \leq t \leq \tau_k^r-1} (w_k^{r,t})^3 \mathbb{E}^r \left[\left\| \mathbf{g}_k^{r,0} \right\|^2 \right]. \quad (44)$$

Applying Assumption 3 to (44):

$$\begin{aligned} & \sum_{t=0}^{\tau_k^r-1} w_k^{r,t} \mathbb{E}^r \left[\left\| \mathbf{g}_k^{r,t} - \mathbf{g}_k^{r,0} \right\|^2 \right] \\ & \leq 8(\tau_k^r)^3 (\eta_k^r)^2 L_k^2 \max_{0 \leq t \leq \tau_k^r-1} (w_k^{r,t})^3 \left(\left\| \nabla_k F(\boldsymbol{\Theta}^{r,0}) \right\|^2 + \sigma_k^2 \right). \end{aligned} \quad (45)$$

Similarly:

$$\begin{aligned} & \sum_{t=0}^{\tau_k^r-1} (w_k^{r,t})^2 \mathbb{E}^r \left[\left\| \mathbf{g}_k^{r,t} - \mathbf{g}_k^{r,0} \right\|^2 \right] \\ & \leq 8(\tau_k^r)^3 (\eta_k^r)^2 L_k^2 \max_{0 \leq t \leq \tau_k^r-1} (w_k^{r,t})^4 \left(\left\| \nabla_k F(\boldsymbol{\Theta}^{r,0}) \right\|^2 + \sigma_k^2 \right). \end{aligned} \quad (46)$$

This completes the proof of Lemma 1. \square

C. Proof of Theorem 1

Applying our smoothness assumption, given in Assumption 1:

$$\begin{aligned} & F(\boldsymbol{\Theta}^{r+1,0}) - F(\boldsymbol{\Theta}^{r,0}) \\ & \leq \left\langle \nabla F(\boldsymbol{\Theta}^{r,0}), \boldsymbol{\Theta}^{r+1,0} - \boldsymbol{\Theta}^{r,0} \right\rangle + \frac{L}{2} \left\| \boldsymbol{\Theta}^{r+1,0} - \boldsymbol{\Theta}^{r,0} \right\|^2 \end{aligned} \quad (47)$$

$$\begin{aligned} & \leq - \sum_{k=0}^K \eta_k^r \sum_{t=0}^{\tau_k^r-1} w_k^{r,t} \left\langle \nabla_k F(\boldsymbol{\Theta}^{r,0}), \mathbf{g}_k^{r,t} \right\rangle \\ & \quad + \frac{L}{2} \sum_{k=0}^K (\eta_k^r)^2 \tau_k^r \sum_{t=0}^{\tau_k^r-1} (w_k^{r,t})^2 \left\| \mathbf{g}_k^{r,t} \right\|^2. \end{aligned} \quad (48)$$

where (48) follows from the fact that $(\sum_{n=1}^N \mathbf{x}_n)^2 \leq N \sum_{n=1}^N \mathbf{x}_n^2$.

We bound the first term in (48):

$$\begin{aligned} & - \left\langle \nabla_k F(\boldsymbol{\Theta}^{r,0}), \mathbf{g}_k^{r,t} \right\rangle \\ & = - \left(\left\langle \nabla_k F(\boldsymbol{\Theta}^{r,0}), \mathbf{g}_k^{r,t} - \mathbf{g}_k^{r,0} \right\rangle + \left\langle \nabla_k F(\boldsymbol{\Theta}^{r,0}), \mathbf{g}_k^{r,0} \right\rangle \right) \end{aligned} \quad (49)$$

$$\begin{aligned} & \leq \frac{1}{2} \left\| \nabla_k F(\boldsymbol{\Theta}^{r,0}) \right\|^2 + \frac{1}{2} \left\| \mathbf{g}_k^{r,t} - \mathbf{g}_k^{r,0} \right\|^2 \\ & \quad - \left\langle \nabla_k F(\boldsymbol{\Theta}^{r,0}), \mathbf{g}_k^{r,0} \right\rangle \end{aligned} \quad (50)$$

where (50) follows from the fact that $A \cdot B = \frac{1}{2}A^2 + \frac{1}{2}B^2 - \frac{1}{2}(A-B)^2 \leq \frac{1}{2}A^2 + \frac{1}{2}B^2$.

We bound the second term in (48):

$$\left\| \mathbf{g}_k^{r,t} \right\|^2 = \left\| \mathbf{g}_k^{r,t} - \mathbf{g}_k^{r,0} + \mathbf{g}_k^{r,0} \right\|^2 \quad (51)$$

$$\leq 2 \left(\left\| \mathbf{g}_k^{r,t} - \mathbf{g}_k^{r,0} \right\|^2 + \left\| \mathbf{g}_k^{r,0} \right\|^2 \right). \quad (52)$$

Plugging (50) and (52) into (48), and applying the expectation \mathbb{E}^r to both sides:

$$\begin{aligned} & \mathbb{E}^r [F(\boldsymbol{\Theta}^{r+1,0})] - F(\boldsymbol{\Theta}^{r,0}) \\ & \leq - \frac{1}{2} \sum_{k=0}^K \eta_k^r \sum_{t=0}^{\tau_k^r-1} w_k^{r,t} (1 - 2\eta_k^r L \tau_k^r w_k^{r,t}) \left\| \nabla_k F(\boldsymbol{\Theta}^{r,0}) \right\|^2 \\ & \quad + \frac{1}{2} \sum_{k=0}^K \eta_k^r \sum_{t=0}^{\tau_k^r-1} w_k^{r,t} \mathbb{E}^r \left[\left\| \mathbf{g}_k^{r,t} - \mathbf{g}_k^{r,0} \right\|^2 \right] \\ & \quad + L \sum_{k=0}^K (\eta_k^r)^2 \tau_k^r \sum_{t=0}^{\tau_k^r-1} (w_k^{r,t})^2 \left(\mathbb{E}^r \left[\left\| \mathbf{g}_k^{r,t} - \mathbf{g}_k^{r,0} \right\|^2 \right] + \sigma_k^2 \right) \end{aligned} \quad (53)$$

$$\begin{aligned} & = - \frac{1}{2} \sum_{k=0}^K \eta_k^r \sum_{t=0}^{\tau_k^r-1} w_k^{r,t} (1 - 2\eta_k^r L \tau_k^r w_k^{r,t}) \left\| \nabla_k F(\boldsymbol{\Theta}^{r,0}) \right\|^2 \\ & \quad + \frac{1}{2} \sum_{k=0}^K \eta_k^r \sum_{t=0}^{\tau_k^r-1} w_k^{r,t} (1 + 2\eta_k^r L \tau_k^r w_k^{r,t}) \mathbb{E}^r \left[\left\| \mathbf{g}_k^{r,t} - \mathbf{g}_k^{r,0} \right\|^2 \right] \\ & \quad + L \sum_{k=0}^K (\eta_k^r)^2 \tau_k^r \sum_{t=0}^{\tau_k^r-1} (w_k^{r,t})^2 \sigma_k^2. \end{aligned} \quad (54)$$

Applying Lemma 1 to (54):

$$\begin{aligned} & \mathbb{E}^r [F(\boldsymbol{\Theta}^{r+1,0})] - F(\boldsymbol{\Theta}^{r,0}) \\ & \leq - \frac{1}{2} \sum_{k=0}^K \eta_k^r \sum_{t=0}^{\tau_k^r-1} w_k^{r,t} (1 - 2\eta_k^r L \tau_k^r w_k^{r,t}) \left\| \nabla_k F(\boldsymbol{\Theta}^{r,0}) \right\|^2 \\ & \quad + 4 \sum_{k=0}^K (\tau_k^r)^3 (\eta_k^r)^2 L_k^2 \max_t (w_k^{r,t})^3 \left(\left\| \nabla_k F(\boldsymbol{\Theta}^{r,0}) \right\|^2 + \sigma_k^2 \right) \\ & \quad + 8L \sum_{k=0}^K (\tau_k^r)^4 (\eta_k^r)^3 L_k^2 \max_t (w_k^{r,t})^4 \left(\left\| \nabla_k F(\boldsymbol{\Theta}^{r,0}) \right\|^2 + \sigma_k^2 \right) \\ & \quad + (\eta_k^r)^2 L \sum_{k=0}^K \tau_k^r \sum_{t=0}^{\tau_k^r-1} (w_k^{r,t})^2 \sigma_k^2. \end{aligned} \quad (55)$$

Let $\eta_k^r \leq \frac{1}{16\tau_k^r \max\{L, L_k\} \max_{0 \leq t \leq \tau_k^r-1} w_k^{r,t}}$. Noticing that $\tau_k^r \leq \sum_{t=0}^{\tau_k^r-1} w_k^{r,t}$, we have:

$$\begin{aligned} & \mathbb{E}^r [F(\Theta^{r+1,0})] - F(\Theta^{r,0}) \\ & \leq -\frac{1}{2} \sum_{k=0}^K \eta_k^r \sum_{t=0}^{\tau_k^r-1} w_k^{r,t} \left(1 - \frac{1}{8} - \frac{1}{32} - \frac{1}{256}\right) \|\nabla_k F(\Theta^{r,0})\|^2 \\ & \quad + L \sum_{k=0}^K (\eta_k^r)^2 \max_{0 \leq t \leq \tau_k^r-1} w_k^{r,t} \tau_k^r \sigma_k^2 \sum_{t=0}^{\tau_k^r-1} w_k^{r,t} \end{aligned} \quad (56)$$

$$\begin{aligned} & \leq -\frac{1}{4} \sum_{k=0}^K \eta_k^r \sum_{t=0}^{\tau_k^r-1} w_k^{r,t} \|\nabla_k F(\Theta^{r,0})\|^2 \\ & \quad + L \sum_{k=0}^K (\eta_k^r)^2 \max_{0 \leq t \leq \tau_k^r-1} w_k^{r,t} \tau_k^r \sigma_k^2 \sum_{t=0}^{\tau_k^r-1} w_k^{r,t}. \end{aligned} \quad (57)$$

After some rearranging of terms:

$$\begin{aligned} & \sum_{k=0}^K \eta_k^r \sum_{t=0}^{\tau_k^r-1} w_k^{r,t} \|\nabla_k F(\Theta^{r,0})\|^2 \\ & \leq 4(F(\Theta^{r,0}) - \mathbb{E}^r [F(\Theta^{r+1,0})]) \\ & \quad + 4L \sum_{k=0}^K (\eta_k^r)^2 \max_{0 \leq t \leq \tau_k^r-1} w_k^{r,t} \tau_k^r \sigma_k^2 \sum_{t=0}^{\tau_k^r-1} w_k^{r,t}. \end{aligned} \quad (58)$$

Next, we average over all global rounds $r = 0, \dots, R-1$ and take total expectation:

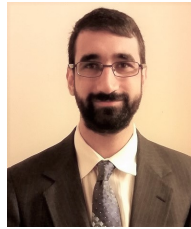
$$\begin{aligned} & \frac{1}{R} \sum_{r=0}^{R-1} \sum_{k=0}^K \eta_k^r \sum_{t=0}^{\tau_k^r-1} w_k^{r,t} \mathbb{E} [\|\nabla_k F(\Theta^{r,0})\|^2] \\ & \leq \frac{4(F(\Theta^{0,0}) - \mathbb{E} [F(\Theta^{R,0})])}{R} \\ & \quad + \frac{4L}{R} \sum_{r=0}^{R-1} \sum_{k=0}^K (\eta_k^r)^2 \max_{0 \leq t \leq \tau_k^r-1} w_k^{r,t} \tau_k^r \sigma_k^2 \sum_{t=0}^{\tau_k^r-1} w_k^{r,t}. \end{aligned} \quad (59)$$

In order to get our weighted averaged on the left-hand side, we divide through by $\sum_{r=0}^{R-1} \sum_{k=0}^K \eta_k^r \sum_{t=0}^{\tau_k^r-1} w_k^{r,t}$, which completes the proof of Theorem 1.

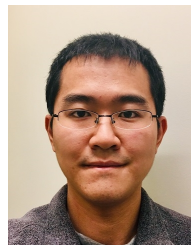
REFERENCES

- [1] P. Voigt and A. Von dem Bussche, "The eu general data protection regulation (GDPR)," *A Practical Guide, 1st Ed., Cham: Springer Int. Publishing*, vol. 10, no. 3152676, pp. 10–5555, 2017.
- [2] "Health insurance portability and accountability act," <https://www.hhs.gov/hipaa/index.html>, accessed June 12, 2020.
- [3] B. McMahan, E. Moore, D. Ramage, S. Hampson, and B. A. y Arcas, "Communication-efficient learning of deep networks from decentralized data," *Proc. 20th Int. Conf. on Artif. Intell.*, pp. 1273–1282, 2017.
- [4] P. Kairouz, H. B. McMahan, B. Avent, A. Bellet, M. Bennis, A. N. Bhagoji, K. A. Bonawitz, Z. Charles, G. Cormode, R. Cummings, R. G. L. D'Oliveira, H. Eichner, S. E. Rouayheb, D. Evans, J. Gardner, C. Garrett, A. Gascón, B. Ghazi, P. B. Gibbons, M. Gruteser, Z. Harchaoui, C. He, L. He, Z. Huo, B. Hutchinson, J. Hsu, M. Jaggi, T. Javidi, G. Joshi, M. Khodak, J. Konečný, A. Korolova, F. Koushanfar, S. Koyejo, T. Lepoint, Y. Liu, P. Mittal, M. Mohri, R. Nock, A. Özgür, R. Pagh, H. Qi, D. Ramage, R. Raskar, M. Raykova, D. Song, W. Song, S. U. Stich, Z. Sun, A. T. Suresh, F. Tramèr, P. Vepakomma, J. Wang, L. Xiong, Z. Xu, Q. Yang, F. X. Yu, H. Yu, and S. Zhao, "Advances and open problems in federated learning," *Found. Trends Mach. Learn.*, vol. 14, no. 1-2, pp. 1–210, 2021.
- [5] Q. Yang, Y. Liu, T. Chen, and Y. Tong, "Federated machine learning: Concept and applications," *ACM Trans. on Intelligent Systems and Technology*, 2019.
- [6] J. Zhou, S. Zhang, Q. Lu, W. Dai, M. Chen, X. Liu, S. Pirttikangas, Y. Shi, W. Zhang, and E. Herrera-Viedma, "A survey on federated learning and its applications for accelerating industrial internet of things," *arXiv:2104.10501*, 2021.
- [7] Y. Liu, Y. Kang, X. Zhang, L. Li, Y. Cheng, T. Chen, M. Hong, and Q. Yang, "A communication efficient vertical federated learning framework," *Adv. Neural Inf. Process. Syst., Workshop on Federated Learning for Data Privacy and Confidentiality*, 2019.
- [8] T. Castiglia, A. Das, S. Wang, and S. Patterson, "Compressed-VFL: Communication-efficient learning with vertically partitioned data," in *Proc. 39th Int. Conf. on Machine Learn.*, 2022, pp. 2738–2766.
- [9] F. Zhou and G. Cong, "On the convergence properties of a k-step averaging stochastic gradient descent algorithm for nonconvex optimization," in *Proc. Int. Joint Conf. Artificial Intelligence*, J. Lang, Ed., 2018, pp. 3219–3227.
- [10] F. Sattler, S. Wiedemann, K. Müller, and W. Samek, "Robust and communication-efficient federated learning from non-i.i.d. data," *IEEE Trans. Neural Networks Learn. Syst.*, vol. 31, no. 9, pp. 3400–3413, 2020.
- [11] Y. Chen, X. Sun, and Y. Jin, "Communication-efficient federated deep learning with layerwise asynchronous model update and temporally weighted aggregation," *IEEE Trans. Neural Networks Learn. Syst.*, vol. 31, no. 10, pp. 4229–4238, 2020.
- [12] H. Jamali-Rad, M. Abdizadeh, and A. Singh, "Federated learning with taskonomy for non-iid data," *IEEE Trans. Neural Netw. Learn. Syst.*, pp. 1–12, 2022.
- [13] C. Sun, L. Ippel, J. van Soest, B. Wouters, A. Malic, O. Adekunle, B. van den Berg, O. Mussmann, A. Koster, C. van der Kallen, C. van Oppen, D. Townend, A. Dekker, and M. Dumontier, "A Privacy-Preserving infrastructure for analyzing personal health data in a vertically partitioned scenario," vol. 264, pp. 373–377, 2019.
- [14] T. Chen, X. Jin, Y. Sun, and W. Yin, "VAFL: a method of vertical asynchronous federated learning," *arXiv:2007.06081*, 2020.
- [15] A. Das, T. Castiglia, S. Wang, and S. Patterson, "Cross-silo federated learning for multi-tier networks with vertical and horizontal data partitioning," *ACM Trans. Intell. Syst. Technol.*, vol. 13, no. 6, 2022.
- [16] Y. Hu, D. Niu, J. Yang, and S. Zhou, "FDML: A collaborative machine learning framework for distributed features," *Proc. 25th ACM Int. Conf. Knowl. Discov. Data Min.*, pp. 2232–2240, 2019.
- [17] F. Fu, X. Miao, J. Jiang, H. Xue, and B. Cui, "Towards communication-efficient vertical federated learning training via cache-enabled local updates," *arXiv:2207.14628*, 2022.
- [18] J. Zhang, S. Guo, Z. Qu, D. Zeng, H. Wang, Q. Liu, and A. Y. Zomaya, "Adaptive vertical federated learning on unbalanced features," *IEEE Trans. Parallel Distributed Syst.*, vol. 33, no. 10, pp. 4006–4018, 2022.
- [19] D. Hazarika, R. Zimmermann, and S. Poria, "MISA: modality-invariant and -specific representations for multimodal sentiment analysis," in *Proc. Int. Conf. Multimedia*, pp. 1122–1131.
- [20] W. Han, H. Chen, and S. Poria, "Improving multimodal fusion with hierarchical mutual information maximization for multimodal sentiment analysis," in *Proc. Conf. Empirical Methods in Natural Language Processing*, 2021, pp. 9180–9192.
- [21] W. Lin, Q. Gao, L. Sun, Z. Zhong, K. Hu, Q. Ren, and Q. Huo, "Vibertgrid: A jointly trained multi-modal 2d document representation for key information extraction from documents," in *16th Int. Conf. Document Analysis and Recognition*, vol. 12821, 2021, pp. 548–563.
- [22] P. Narkhede, R. Walambe, S. Mandaokar, P. Chandel, K. Kotecha, and G. Ghinea, "Gas detection and identification using multimodal artificial intelligence based sensor fusion," *Applied System Innovation*, vol. 4, p. 3, 2021.
- [23] A. Reisizadeh, H. Taheri, A. Mokhtari, H. Hassani, and R. Pedarsani, "Robust and communication-efficient collaborative learning," *Adv. Neural Inf. Process. Syst.*, pp. 8386–8397, 2019.
- [24] Z. Xu, Z. Yang, J. Xiong, J. Yang, and X. Chen, "ELFISH: resource-aware federated learning on heterogeneous edge devices," *arXiv:1912.01684*, 2019.
- [25] A. Reisizadeh, I. Tziotis, H. Hassani, A. Mokhtari, and R. Pedarsani, "Straggler-resilient federated learning: Leveraging the interplay between statistical accuracy and system heterogeneity," *arXiv:2012.14453*, 2020.
- [26] Q. Zhang, B. Gu, C. Deng, and H. Huang, "Secure bilevel asynchronous vertical federated learning with backward updating," in *Proc. Conf. Artif. Intel.*, 2021, pp. 10 896–10 904.

- [27] H. Shi, Y. Xu, Y. Jiang, H. Yu, and L. Cui, "Efficient asynchronous multi-participant vertical federated learning," *IEEE Trans. on Big Data*, pp. 1–12, 2022.
- [28] H. Cui, H. Zhang, G. R. Ganger, P. B. Gibbons, and E. P. Xing, "GeePS: scalable deep learning on distributed GPUs with a GPU-specialized parameter server," *Proc. 11th Eur. Conf. Comput. Syst.*, pp. 4:1–4:16, 2016.
- [29] W. Dai, "Learning with staleness," Ph.D. dissertation, 2018.
- [30] V. Mugunthan, P. Goyal, and L. Kagal, "Multi-VFL: A vertical federated learning system for multiple data and label owners," *arXiv:2106.05468*, 2021.
- [31] K. Yang, Z. Song, Y. Zhang, Y. Zhou, X. Sun, and J. Wang, "Model optimization method based on vertical federated learning," *IEEE Int. Symp. on Circuits Syst.*, pp. 1–5, 2021.
- [32] B. Gu, A. Xu, Z. Huo, C. Deng, and H. Huang, "Privacy-preserving asynchronous vertical federated learning algorithms for multiparty collaborative learning," *IEEE Trans. Neural Netw. Learn. Syst.*, pp. 1–13, 2021.
- [33] Q. Zhang, B. Gu, C. Deng, S. Gu, L. Bo, J. Pei, and H. Huang, "Asysqn: Faster vertical federated learning algorithms with better computation resource utilization," in *ACM Conf. Knowl. Disc. Data Mining*, 2021, pp. 3917–3927.
- [34] C. Xie, P. Chen, C. Zhang, and B. Li, "Improving privacy-preserving vertical federated learning by efficient communication with ADMM," *arXiv:2207.10226*, 2022.
- [35] J. Wang, Q. Liu, H. Liang, G. Joshi, and H. V. Poor, "A novel framework for the analysis and design of heterogeneous federated learning," *IEEE Trans. Signal Process.*, vol. 69, pp. 5234–5249, 2021.
- [36] T. Li, A. K. Sahu, M. Zaheer, M. Sanjabi, A. Talwalkar, and V. Smith, "Federated optimization in heterogeneous networks," *Proc. of Machine Learn. Sys.*, 2020.
- [37] A. Koloskova, N. Loizou, S. Boreiri, M. Jaggi, and S. Stich, "A unified theory of decentralized SGD with changing topology and local updates," *Int. Conf. of Machine Learn.*, vol. 119, pp. 5381–5393, 2020.
- [38] T. Castiglia, A. Das, and S. Patterson, "Multi-level local SGD: Distributed SGD for heterogeneous hierarchical networks," *Int. Conf. on Learn. Representations*, 2021.
- [39] J. Bradley, A. Kyrola, D. Bickson, and C. Guestrin, "Parallel coordinate descent for ℓ_1 -regularized loss minimization," *Int. Conf. Machine Learn.*, 2011.
- [40] J. Liu, S. Wright, C. Ré, V. Bittorf, and S. Sridhar, "An asynchronous parallel stochastic coordinate descent algorithm," *Int. Conf. Machine Learn.*, 2014.
- [41] P. Richtárik and M. Takác, "Distributed coordinate descent method for learning with big data," *J. Machine Learn. Res.*, 2016.
- [42] L. Wan, W. K. Ng, S. Han, and V. Lee, "Privacy-preservation for gradient descent methods," *Proc. 13th ACM Int. Conf. Knowl. Discov. Data Min.*, pp. 775–783, 2007.
- [43] S. Yang, B. Ren, X. Zhou, and L. Liu, "Parallel distributed logistic regression for vertical federated learning without third-party coordinator," *arXiv:1911.09824*, 2019.
- [44] S. Hardy, W. Henecka, H. Ivey-Law, R. Nock, G. Patrini, G. Smith, and B. Thorne, "Private federated learning on vertically partitioned data via entity resolution and additively homomorphic encryption," *arXiv:1711.10677*, 2017.
- [45] L. Bottou, F. E. Curtis, and J. Nocedal, "Optimization methods for large-scale machine learning," *SIAM Review*, vol. 60, no. 2, pp. 223–311, 2018.
- [46] J. Tsitsiklis, D. Bertsekas, and M. Athans, "Distributed asynchronous deterministic and stochastic gradient optimization algorithms," *IEEE Trans. Autom. Control*, vol. 31, no. 9, pp. 803–812, 1986.
- [47] L. M. Nguyen, P. H. Nguyen, M. van Dijk, P. Richtárik, K. Scheinberg, and M. Takác, "SGD and Hogwild! convergence without the bounded gradients assumption," *Proc. 35th Int. Conf. on Machine Learn.*, vol. 80, pp. 3747–3755, 2018.
- [48] L. T. Phong, Y. Aono, T. Hayashi, L. Wang, and S. Moriai, "Privacy-preserving deep learning via additively homomorphic encryption," *IEEE Trans. Inf. Forensics Security*, vol. 13, no. 5, pp. 1333–1345, 2018.
- [49] J. Geiping, H. Bauermeister, H. Dröge, and M. Moeller, "Inverting gradients - how easy is it to break privacy in federated learning?" *Adv. Neural Inf. Process. Syst.*, 2020.
- [50] A. Mahendran and A. Vedaldi, "Understanding deep image representations by inverting them," *Proc. IEEE Int. Conf. Comput. Vis.*, pp. 5188–5196, 2015.
- [51] K. Cheng, T. Fan, Y. Jin, Y. Liu, T. Chen, and Q. Yang, "Secureboost: A lossless federated learning framework," *IEEE Intelligent Systems*, vol. 36, no. 6, pp. 87–98, 2021.
- [52] S. Ghadimi and G. Lan, "Stochastic first- and zeroth-order methods for nonconvex stochastic programming," *SIAM J. Optim.*, vol. 23, no. 4, pp. 2341–2368, 2013.
- [53] A. Zadeh, P. P. Liang, S. Poria, E. Cambria, and L. Morency, "Multimodal language analysis in the wild: CMU-MOSEI dataset and interpretable dynamic fusion graph," *Proc. 56th Annu. Meet. Assoc. Comput. Linguist.*, pp. 2236–2246, 2018.
- [54] J. Deng, W. Dong, R. Socher, L.-J. Li, K. Li, and L. Fei-Fei, "Imagenet: A large-scale hierarchical image database," in *IEEE Conference on Computer Vision and Pattern Recognition*, 2009.
- [55] Z. Wu, S. Song, A. Khosla, F. Yu, L. Zhang, X. Tang, and J. Xiao, "3D shapenets: A deep representation for volumetric shapes," *Proc. IEEE Int. Conf. Comput. Vis.*, pp. 1912–1920, 2015.
- [56] V. Smith, S. Forte, C. Ma, M. Takác, M. I. Jordan, and M. Jaggi, "CoCoA: A general framework for communication-efficient distributed optimization," *J. Machine Learn. Res.*, vol. 18, pp. 230:1–230:49, 2017.
- [57] C. Reiss, J. Wilkes, and J. L. Hellerstein, "Google cluster-usage traces: format + schema," Google Inc., Technical Report, 2011.
- [58] T. Lin, S. U. Stich, K. K. Patel, and M. Jaggi, "Don't use large mini-batches, use local SGD," *Int. Conf. on Learn. Representations*, 2020.



Timothy Castiglia is a field consultant at Ab Initio Software. He received his Ph.D. degree from the Department of Computer Science at Rensselaer Polytechnic Institute, Troy, NY, USA. He received his B.S. degree in Computer Science in 2017 from the same institute. His research interests include distributed systems, machine learning, and network science.



Shiqiang Wang (S'13–M'15–SM'23) received his Ph.D. from the Department of Electrical and Electronic Engineering, Imperial College London, United Kingdom, in 2015. He is currently a Staff Research Scientist at IBM T. J. Watson Research Center, NY, USA. His current research focuses on the intersection of distributed computing, machine learning, networking, and optimization, with a broad range of applications including data analytics, edge-based artificial intelligence (Edge AI), Internet of Things (IoT), and future wireless systems. He has made foundational contributions to edge computing and federated learning that generated both academic and industrial impact. Dr. Wang serves as an associate editor of the IEEE Transactions on Mobile Computing and IEEE Transactions on Parallel and Distributed Systems. He received the IEEE Communications Society (ComSoc) Leonard G. Abraham Prize in 2021, IEEE ComSoc Best Young Professional Award in Industry in 2021, IBM Outstanding Technical Achievement Awards (OTAA) in 2019, 2021, 2022, and 2023, multiple Invention Achievement Awards from IBM since 2016, Best Paper Finalist of the IEEE International Conference on Image Processing (ICIP) 2019, and Best Student Paper Award of the Network and Information Sciences International Technology Alliance (NIS-ITA) in 2015.



Stacy Patterson is an Associate Professor in the Department of Computer Science at Rensselaer Polytechnic Institute. She received the MS and PhD in computer science from UC Santa Barbara in 2003 and 2009, respectively. From 2009–2011, she was a postdoctoral scholar at the Center for Control, Dynamical Systems and Computation at UC Santa Barbara. From 2011–2013, she was a postdoctoral fellow in the Department of Electrical Engineering at Technion - Israel Institute of Technology. Dr. Patterson is the recipient of a Viterbi postdoctoral fellowship, the IEEE CSS Axelby Outstanding Paper Award, and an NSF CAREER award. Her research interests include distributed systems, cloud computing, and the Internet of Things.